nature medicine

Article

https://doi.org/10.1038/s41591-022-02073-x

# Inhaled particulate accumulation with age impairs immune function and architecture in human lung lymph nodes

Received: 14 November 2021

Accepted: 3 October 2022

Published online: 21 November 2022

Check for updates

Basak B. Ural[1], Daniel P. Caron[1], Pranay Dogra[1], Steven B. Wells[2], Peter A. Szabo[1], Tomer Granot[3], Takashi Senda[4], Maya M. L. Poon[1], Nora Lam[1], Puspa Thapa[1], Yoon Seung Lee[1], Masaru Kubota[4], Rei Matsumoto[4] & Donna L. Farber[1,4]

Older people are particularly susceptible to infectious and neoplastic diseases of the lung and it is unclear how lifelong exposure to environmental pollutants affects respiratory immune function. In an analysis of human lymph nodes (LNs) from 84 organ donors aged 11–93 years, we found a specific age-related decline in lung-associated, but not gut-associated, LN immune function linked to the accumulation of inhaled atmospheric particulate matter. Increasing densities of particulates were found in lung-associated LNs with age, but not in the corresponding gut-associated LNs. Particulates were specifically contained within $CD68^{+}CD169^{-}$ macrophages, which exhibited decreased activation, phagocytic capacity, and altered cytokine production compared with non-particulate-containing macrophages. The structures of B cell follicles and lymphatic drainage were also disrupted in lung-associated LNs with particulates. Our results reveal that the cumulative effects of environmental exposure and age may compromise immune surveillance of the lung via direct effects on immune cell function and lymphoid architecture.

The demographics of the world population are rapidly changing, such that it has been projected that individuals 65 years or older will represent over 20% of the population by 2050[1]. As the majority of healthcare costs, morbidity and mortality from diseases are experienced by individuals over 55 years of age[2], there is a need to better understand the mechanisms by which aging increases disease susceptibility. In particular, there is a significant and striking increase in both the incidence and severity of diseases of the lung and respiratory tract with age. Older people are at increased risk for lung damage, as well as severe outcomes from infection with respiratory viruses such influenza[3] and severe acute respiratory syndrome coronavirus 2 (SARS-CoV-2), for which mortality from infection in individuals >75 years is more than 80-fold greater than in younger adults[4–6]. Moreover, neoplastic disease of the lung, including small cell lung cancer, mostly affects individuals older than 60 years[7].

Senescent changes in the immune system have been implicated in the increased disease burden in older people. With age, immune cells and functional mediators undergo intrinsic alterations leading to decreased adaptive immune responses, increased inflammation[8,9] and decreased regulation[10], thus impairing anti-pathogen and anti-tumor immunity. However, the mechanisms for the biased decline in respiratory immunity over age are not known. In addition, aging and its effects on the respiratory tract are shaped by prolonged exposure to the environment through inhalation[11,12], although the role of environmental

[1]Department of Microbiology and Immunology, Columbia University Irving Medical Center, New York, NY, USA. [2]Department of Systems Biology, Columbia University Irving Medical Center, New York, NY, USA. [3]Columbia Center for Translational Immunology, Columbia University, New York, NY, USA. [4]Department of Surgery, Columbia University Irving Medical Center, New York, NY, USA. e-mail: df2396@cumc.columbia.edu

https://doi.org/10.1038/s41591-022-02073-x

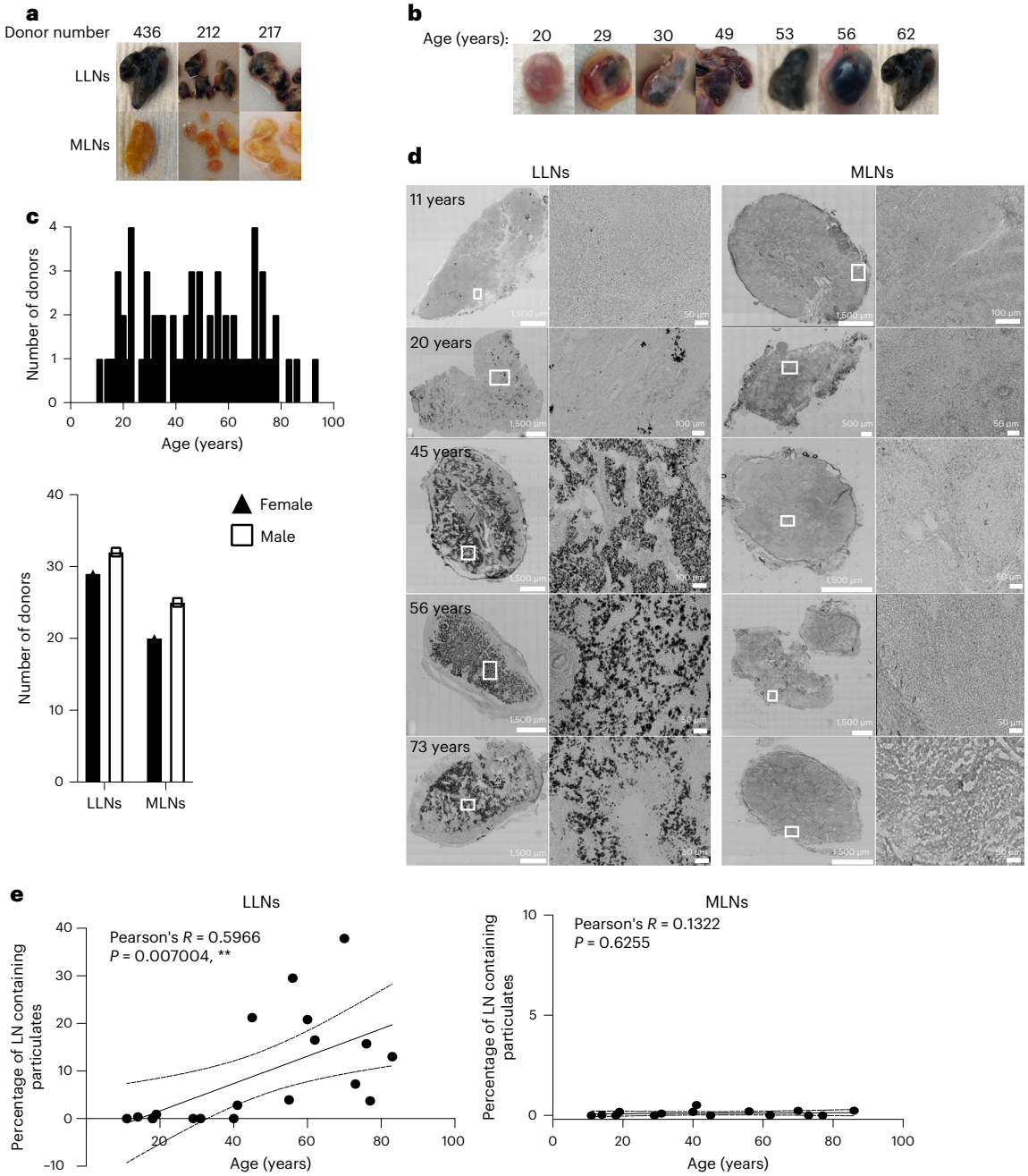


**Fig. 1 | LLNs accumulate carbon particulates with age. a**, Photos showing the gross anatomy of LLNs (top) and gut-associated MLNs (bottom) dissected from lung and intestine samples. **b**, Appearance of whole LLNs by age. **c**, Graphs of the donors whose samples were used in this study, stratified by age (top) and sex for each site (bottom). **d**, Brightfield confocal images of human LLNs (left) and MLNs (right). For each site, the left column shows whole LN sections stitched together from 70–400 single 20× images and the right column shows magnified sections, as outlined by the white boxes in the images to the left. The ages of the organ donors are indicated. The black regions show particulate contents. Representative images were taken from 5–7 donors (LLNs) and 4–6 donors (MLNs) per age group (≤39, 40–64 and ≥65 years). Scale bars, 1,500 µm (whole sections except for MLN from 20 yr old donor which is 500 µm) and 100 or 50 µm (single images). **e**, Particulate content in LNs, quantified by measuring the area (µm$^2$) of each LN that contained black particulates. Imaging data were quantified using Imaris software. Linear regression was performed with Pearson's correlation (two tailed). *P* values and Pearson's *R* values are provided (**, p<0.01). The data are presented as means ± 95% CIs. The data are from 16–19 donors per site.

insults in age-associated impairments of the immune system is not well understood.

Studies of immunosenescence in humans sample blood as the most accessible site. However, immune responses occur in mucosal and barrier sites of infection and associated lymphoid organs. For responses to respiratory infections, lung-associated lymph nodes (LLNs) are crucial for adaptive immune responses to new and recurring pathogens, as demonstrated in mouse models[13,14]. Antigens encountered in the lungs enter LLNs via lymphatics where adaptive immune responses are initiated, including T cell priming and interactions with B cells in specialized lymphoid follicles to promote humoral immunity. Age-associated effects on LNs have been identified in mice[15] and morphological changes with age have been reported in human LNs[16,17]; however, analysis of human LN aging and its effect on immune responses and functionality has not been performed. As part of their role in immune surveillance, LNs also filter impurities from tissues

https://doi.org/10.1038/s41591-022-02073-x

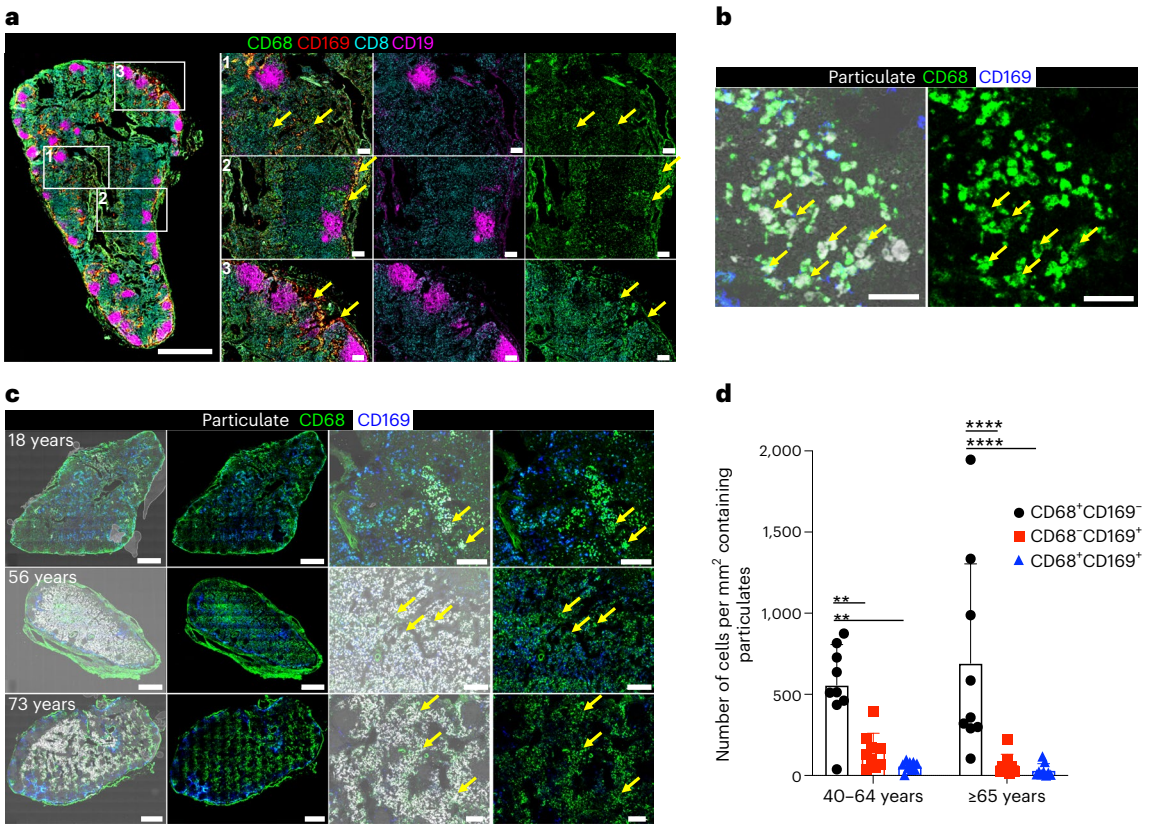


**Fig. 2 | The CD68$^+$CD169$^-$ subset of LN macrophages localize within the T cell zone and contain particulates. a**, Confocal images of LLNs immunostained for CD68 (green), CD169 (red), CD8 (cyan) and CD19 (magenta). Left, whole LN section stitched together from 70–400 single 20× images. Right, magnified sections as outlined by the white boxes to the left. Each row of magnified images shows the localization of a different macrophage subset (1 = CD68$^+$CD169$^-$; 2 = CD68$^+$CD169$^+$; 3 = CD68$^-$CD169$^+$). Representative cells for each subset indicated with yellow arrow. Scale bars, 2,000 µm (whole LN section) and 200 µm (single images). **b**, Confocal images of human LLNs stained for CD68 and CD169 to show macrophage subsets and black particulate matter localization (brightfield microscopy; white). Yellow arrows indicate the representative CD68$^+$CD169$^-$ macrophages containing particulate matter. Representative images were taken from six donors. Scale bars, 50 µm. **c**, Confocal images of human LLNs stained for CD68 and CD169 to show black particulate matter accumulation in different macrophage subsets of the indicated ages. The left two columns show whole LN sections stitched together from 70–400 single 20× images. The right two columns show magnified sections. Within these sets of images, the left columns show a brightfield imaging overlay to indicate the localization of particulates (white). Yellow arrows indicate the representative CD68$^+$CD169$^-$ macrophages containing particulate matter. Representative images were taken from 6–9 donors per age group (≤39, 40–64 and ≥65 years). Scale bars, 1,000 µm (whole LN sections) and 200 µm (single images). **d**, Bar graph showing the macrophage subsets that contained particulates (<3 µm) for different age groups, as calculated using Imaris software. The data are presented as means ± s.d. and are from 18 donors. Statistical significance was determined by two-way ANOVA with Tukey's post-hoc test. Statistically significant differences were found for the following comparisons: $P = 0.0012$ (**, p<0.01) for CD68$^+$CD169$^-$ versus CD68$^+$CD169$^+$ at 40–64 years, $P = 0.0083$ (**) for CD68$^+$CD169$^-$ versus CD68$^-$CD169$^+$ at 40–64 years, $P < 0.0001$(****) for CD68$^+$CD169$^-$ versus CD68$^+$CD169$^+$ at ≥65 years and $P < 0.0001$(****) for CD68$^+$CD169$^-$ versus CD68$^-$CD169$^+$ at ≥65 years.

through lymphatics[18,19], although the impact of this broader role for LNs on human immune responses remains unexplored. Here, we took an anatomical approach to investigate the cellular, structural and functional niches of tissue-draining LNs in samples from human organ donors of different ages, revealing localized, age-associated changes in LLNs due to the accumulation of inhaled atmospheric particulates from environmental pollutants.

## Results

### Atmospheric particulates accumulate in LLNs

We obtained multiple LN samples associated with lungs and intestines from human organ donors (see Methods), through a human tissue resource we established involving collaborations with organ procurement organizations, as previously described[20]. Based on our acquisition of tissues from hundreds of organ donors of all ages (with no history of smoking) over the past decade[21–25], we consistently observed differences in the appearance of LNs associated with the lung and gut, respectively. Here, we show that LLNs are black in color, while mesenteric LNs (MLNs) from the same individual are beige or translucent in color (Fig. 1a), similar to mouse LNs. Comparing LNs from donors of different ages revealed that black LLNs were observed in the majority of adult donors after the third decade of life but were less prevalent in younger donors (<30 years) (Fig. 1b). Black particulates are present in the atmosphere and consist of different polycyclic aromatic hydrocarbons derived from environmental pollutants such as motor vehicle exhausts, heating and wildfires[12,26]. We therefore hypothesized that inhaled atmospheric particulates and their accumulation with age may result in specific alterations to the immune function and architecture of LLNs.

We took a quantitative imaging approach to assess the impact of age and inhaled particulates on LN structure and function in LLNs and MLNs from a cohort of 84 organ donors aged 11–93 years, distributed equally between males and females, with no documented history of heavy smoking (>20 packs for 1 year or longer; see Methods for criteria) (Fig. 1c and Extended Data Table 1). We imaged whole LN sections by confocal microscopy, stitching together multiple (70–400)

https://doi.org/10.1038/s41591-022-02073-x

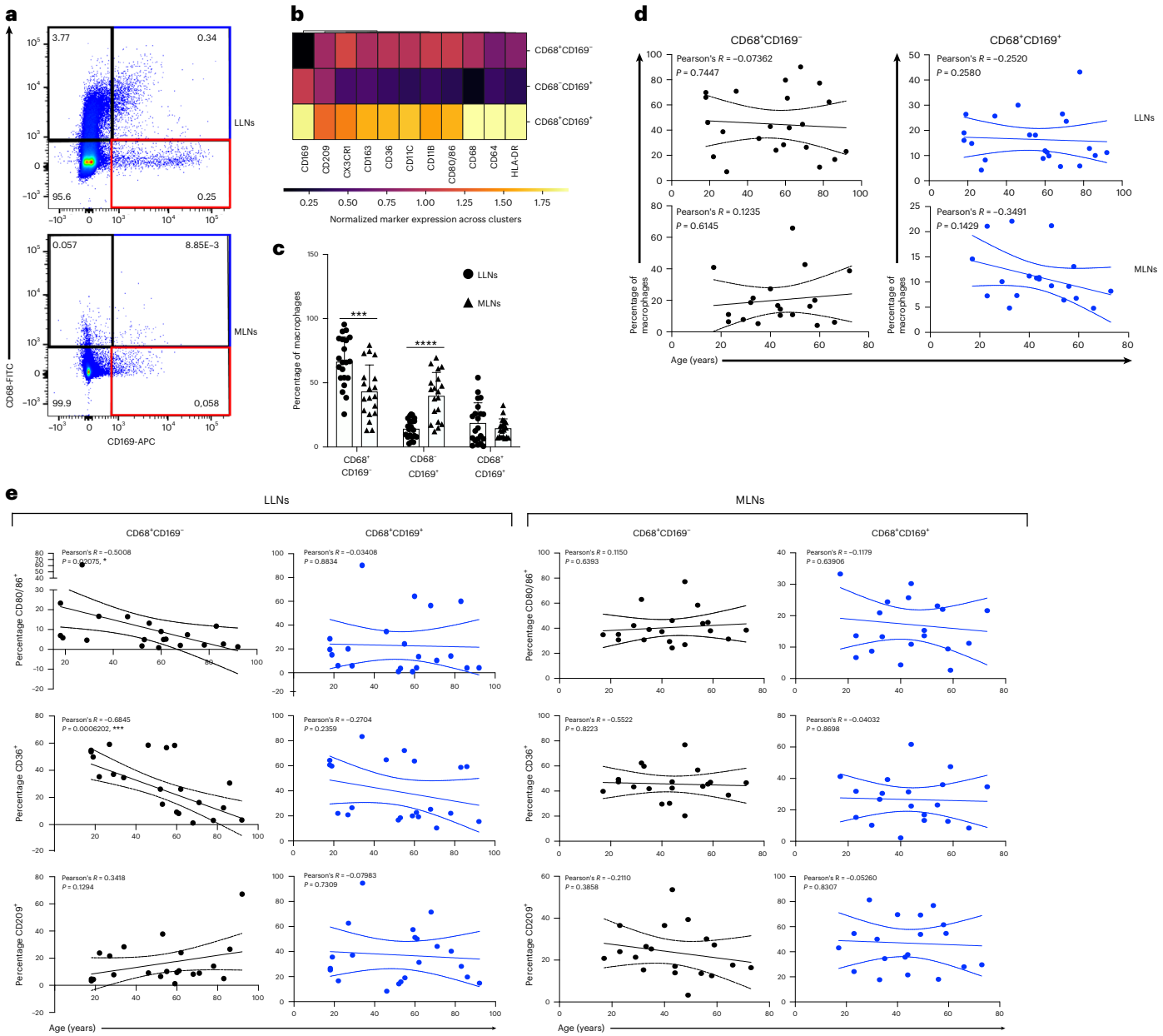


**Fig. 3 | Particulate-containing CD68$^+$CD169$^-$ macrophages are increased in LLNs and exhibit decreasing function with age. a**, Expression of CD68 and CD169 gated on live, singlet and CD45$^+$CD3$^-$ cells, showing CD68$^+$CD169$^-$ (black rectangle), CD68$^-$CD169$^+$ (red rectangle) and CD68$^+$CD169$^+$ (blue rectangle) macrophage subsets. **b**, Heat map showing the differential expression of the indicated markers by the three macrophage subsets, compiled from LLNs. **c**, Frequency of macrophage subsets in LLNs ($n = 21$) and MLNs ($n = 19$). Statistical significance was determined by mixed-effects analysis with Tukey's post-hoc test. The data are presented as means ± s.d. Statistically significant differences between macrophage subset frequencies in LLNs versus MLNs were found for CD68$^+$CD169$^-$ (P=0.0004,*** for p<0.001) and CD68$^-$CD169$^+$(<0.0001,****) cells. There was no significant difference ($P = 0.9458$) for CD68$^+$CD169$^+$cells. **d**, Frequency of macrophage subsets in LLNs ($n = 21$) and MLNs ($n = 19$) by age. Linear regression was performed with Pearson's correlation (two tailed). *P* values and Pearson's *R* values are provided (n.s.). The data are presented as means ± 95% CIs. **e**, Expression of the functional markers CD80/86, CD36 and CD209 by CD68$^+$CD169$^-$ and CD68$^+$CD169$^+$ macrophage subsets in LLNs ($n = 22$) and MLNs ($n = 21$) by age. Linear regression was performed with Pearson's correlation (two tailed). *P* values and Pearson's *R* values are provided (*, p<0.05, ***, p<0.001). The data are presented as means ± 95% CIs.

20× single images (see Methods) to quantify the structural and cellular changes between sites and with age. Brightfield images showed increased particulate matter with age, specifically in LLNs, which was most notable at 40 years of age and older, while MLNs from each corresponding donor did not exhibit particulates at any age (Fig. 1d,e). This age-related accumulation of atmospheric particulates in LLNs was similar between males and females (Extended Data Fig. 1), suggesting environmental effects localized to the LLNs draining the respiratory tract, irrespective of sex.

## Uptakes of particulates by CD68$^+$CD169$^-$ macrophages in LLNs

LNs comprise densely packed immune cells that are organized in defined structural niches. B cells are organized in follicles that in humans are arranged in the periphery and throughout the organ (Fig. 2a, magenta), while CD8$^+$ T cells are situated around and outside follicles delineating the T cell zone (Fig. 2a, cyan). LN macrophages, as defined in mouse models, are subdivided into different subsets based on their localization within the T cell zone, the subcapsular region or follicles[27,28]. To define macrophage populations and their localization in human LNs,

https://doi.org/10.1038/s41591-022-02073-x

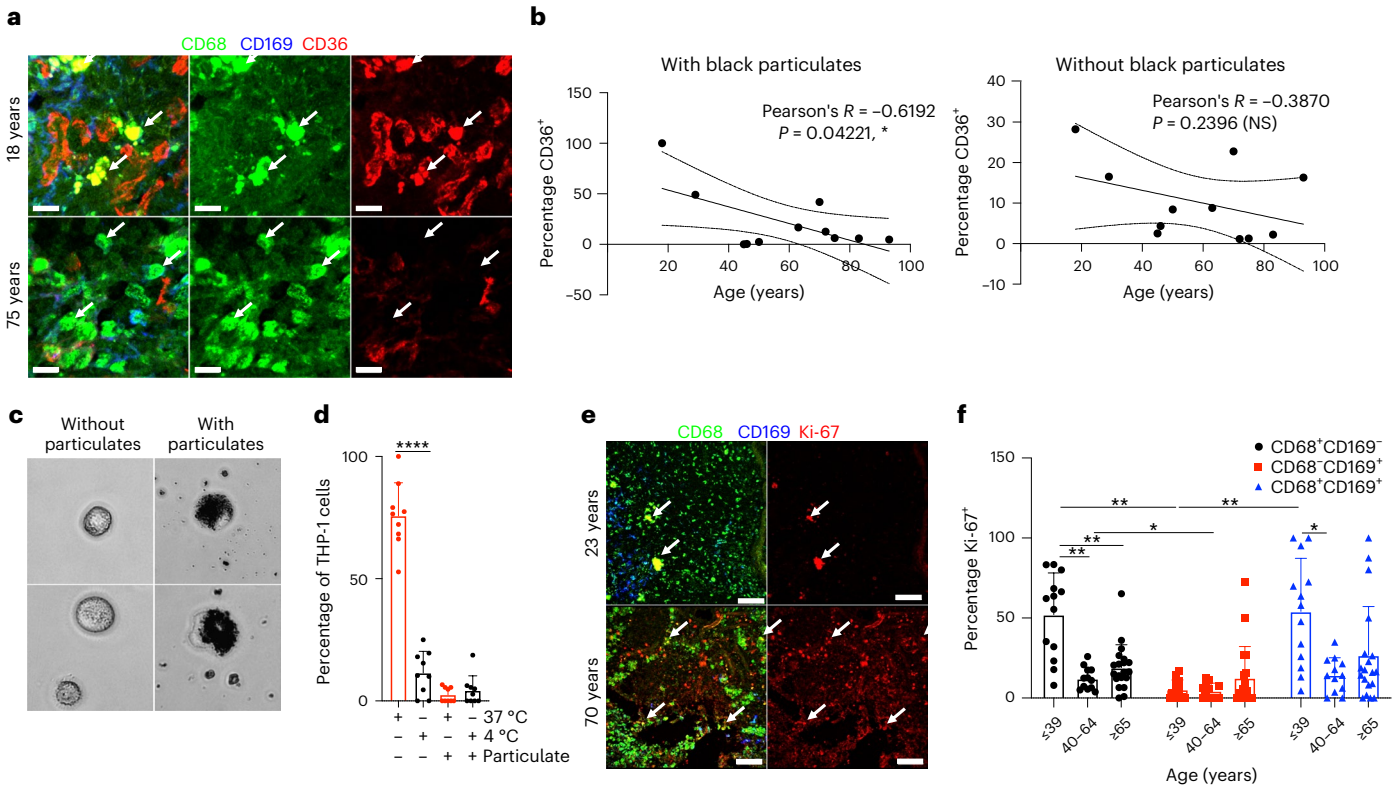


**Fig. 4 | Particulate-containing CD68$^+$CD169$^-$ macrophages have diminished phagocytosis. a**, Confocal images of human LLNs stained for CD68, CD36 and CD169 from donors of the indicated ages. The white arrows show CD68$^+$CD169$^-$ macrophages and CD36 expression in LNs from a representative young and older donor. Representative images were taken from 5–6 donors per age group (≤65 and ≥65 years). Scale bars, 15 µm. **b**, Graphs showing the frequency of CD36$^+$ CD68$^+$CD169$^-$ macrophages by age and stratified by those with (left) or without (right) black particulates ($n = 11$). The calculations were made using Imaris software. Linear regression was performed with Pearson correlation (two tailed). $P$ values and Pearson's $R$ values are provided (*, p<0.05). The data are presented as means ± 95% CIs. NS, not significant. **c**, THP-1 macrophages phagocytose black particulates. Differentiated THP-1 cells were incubated with or without black particulates for 6 h. The representative images show black particulates (≥4 µm size) within macrophages ($n = 3$ wells per condition; three images per well). **d**, Particulate-containing THP-1 macrophages exhibit decreased phagocytosis. Differentiated THP-1 cells previously incubated with or without black particulates were cultured with pHrodo beads at 37 or 4 °C for 90 min and phagocytic uptake was determined by confocal microscopy (2–3 images per well). The graph shows the frequency of THP-1 cells containing beads for each well and condition, representative of two experiments ($n = 9$–12 wells per condition). Statistical significance between phagocytosis by THP-1 cells without or with particulates was determined by one-way ANOVA with Tukey's post-hoc test (****$P < 0.0001$). **e**, Differential proliferation of macrophages in LLNs by age. Confocal images of human LLNs stained for CD68, Ki-67 and CD169 are presented. The white arrows show Ki-67$^+$ macrophages. Representative images were taken from 6–7 donors (2–4 images per donor) per age group (≤65 and ≥65 years). Scale bars, 100 µm. **f**, Graph showing the frequency of proliferating (Ki-67$^+$) cells for each macrophage subset and for different age groups, as calculated using Imaris software. Statistical significance was determined by mixed-effects analysis with Tukey's post-hoc test. Statistically significant differences were found for the following comparisons: $P = 0.004$ (**) for CD68$^+$CD169$^-$ at ≤39 years versus CD68$^+$CD169$^-$ at 40–64 years, $P = 0.0095$ (**) for CD68$^+$CD169$^-$ at ≤39 years versus CD68$^+$CD169$^-$ at ≥65 years, $P = 0{\cdot}0373$(*) for CD68$^+$CD169$^-$ at 40–64 years versus CD68$^-$CD169$^+$ at 40–64 years, $P = 0.0023$ (**) for CD68$^+$CD169$^-$ at ≤39 years versus CD68$^-$CD169$^+$ at ≤39 years, $P = 0.0071$(**) for CD68$^-$CD169$^+$ at ≤39 years versus CD68$^+$CD169$^+$ at ≤39 years and P = 0.0384 (*) for CD68$^+$CD169$^+$ at ≤39 years versus CD68$^+$CD169$^+$ at 40–64 years. The data are presented as means ± s.d. and are from 13 donors (2–7 single images per donor).

we stained LN sections with CD68 (a scavenger receptor expressed by tissue or migratory macrophages[29]) and CD169 (a sialic acid receptor expressed by tissue-resident and subcapsular macrophages in mucosal and lymphoid sites, respectively[30–32]). In human LNs, we observed CD68$^+$ macrophages distributed within the T cell zone and in the subcapsular region around follicles (Fig. 2a, regions 1 and 2), while CD169 expression distinguished subcapsular and medullary from T cell zone macrophages (TCZMs) (Fig. 2a; compare regions 1, 2 and 3). Three subsets of macrophages could be distinguished based on coordinate expression of CD68 and CD169: CD68$^+$CD169$^-$ macrophages were mostly found in the T cell zone (Fig. 2a, region 1, green); CD68$^+$CD169$^+$ macrophages were in the subcapsular sinus (region 2, yellow); and CD68$^-$CD169$^+$ macrophages were in the medullary sinus (region 3, red). Human LNs therefore contain macrophages distributed in all regions, with specific subsets in T cell zones and subcapsular regions.

We hypothesized that particulates would be contained within innate immune cells with the capacity to engulf foreign antigens through phagocytosis. In LNs, phagocytic cells mostly comprise macrophages and/or dendritic cells, as neutrophils and monocytes are not significantly represented in LNs[21,23]. Comparison of brightfield images (particulates) with fluorescence staining of lineage markers in LNs revealed that particulates are contained within macrophages (CD68$^+$ cells) and not within dendritic cells (CD11c$^+$HLA-DR$^+$CD141$^+$ cells) (Fig. 2b and Extended Data Fig. 2a). We further investigated whether particulates were contained within specific macrophages subsets. Using quantitative imaging analysis of whole LNs, we found that the majority of particulates were contained within CD68$^+$CD169$^-$ macrophages (Fig. 2c,d), which also expressed CD11c (Extended Data Fig. 2b,c)—a phenotypic feature of TCZMs in mice[27,33]. We did not find significant particulates in subcapsular (CD68$^+$CD169$^+$) and medullary (CD68$^-$CD169$^+$) macrophages. Together, these results suggest that TCZMs are the predominant subset containing particulate matter within LNs, consistent with the role of this subset as scavengers for dying and dead cells[33].

### Particulates impair macrophage phagocytosis and turnover

In tissues, macrophages are strategically localized to serve as a gatekeeper to phagocytose pathogens, dead cells or debris. We investigated whether the increased presence of particulates with age in TCZMs in LLNs would result in altered activation, phagocytic capacity and/or turnover. We used flow cytometry to assess markers of activation and phagocytosis for macrophage subsets in LLNs and MLNs of organ donors aged 18–92 years, to control for the effects of subset, site, age and particulate content. The flow cytometry panel for analysis contained markers for lineage (CD64, CD68 (refs. [29,34]), CD11c and CD11b) tissue residence (CD163 (ref. [35]), CD169 (refs. [30–32]) and CX3CR1 (refs. [36,37])), activation (HLA-DR, CD80 and CD86) and phagocytosis, including the scavenger receptor CD36, which is important for the uptake of apoptotic cells and bacteria[38], and CD209 (DC-SIGN1), a marker of phagocytic capacity for pathogens[39].

Consistent with our imaging data, three major macrophage subsets were delineated based on CD68 and CD169 expression (Fig. 3a and Extended Data Fig. 3 (gating strategy)); each subset differed in the expression of phenotypic markers for macrophage subsets (CD64, CD11c, CD11b, CD163 and CX3CR1), localization (CX3CR1) and function (CD209, HLA-DR, CD36 and CD80/86) (Fig. 3b). We identified differences in the composition of macrophage subsets between LLNs and MLNs; there was an increased frequency of $CD68^+CD169^-$ macrophages in LLNs compared with MLNs and the frequency of these subsets at each site did not change with age (Fig. 3c,d and Extended Data Fig. 4a). However, expression of the key activation markers CD80 and CD86 and the phagocytic marker CD36 decreased with age specifically in $CD68^+CD169^-$ macrophages in LLNs but not in MLNs (Fig. 3e), nor in $CD68^+CD169^+$ subcapsular and $CD68^-CD169^+$ medullary sinus macrophages in either LLNs or MLNs (Fig. 3e and Extended Data Fig. 4b). In contrast, CD209 expression was not altered significantly with age in any macrophage subset at either site (Fig. 3e and Extended Data Fig. 4b). These results show that while the frequencies of LN macrophage subsets are largely maintained as age progresses, the expression of functional markers specifically in the $CD68^+CD169^-$ subset within LLNs decreases with age, suggesting that particulates may have specific effects on macrophage function.

We investigated the direct effect of particulates on phagocytic capacity by imaging and functional assays. The decrease in CD36 expression with age in LLN $CD68^+CD169^-$ macrophages, as measured by flow cytometry, was also observed by imaging (Fig. 4a), and specifically in $CD68^+CD169^-$ macrophages containing particulates but not in $CD68^+CD169^-$ macrophages without particulates (Fig. 4b). To directly assess whether particulate uptake by macrophages inhibits phagocytosis, we performed phagocytic assays using the THP-1 human macrophage cell line exposed to carbon particulates isolated from urban environmental sources (see Methods). THP-1 cells readily take up these atmospheric black particulates within 6 h (Fig. 4c), demonstrating the efficiency of macrophage-mediated surveillance. Using an in vitro phagocytic assay for the uptake of fluorescent bioparticles consisting of bacteria with a pH-sensitive dye that fluoresces when phagocytosed (see Methods), we found a significant decrease in phagocytosis by particulate-containing compared with non-particulate-containing THP-1 cells (Fig. 4d and Extended Data Fig. 5a). These results show that particulate uptake by macrophages can directly impact the phagocytic function of macrophages that are important for scavenging and the maintenance of tissue homeostasis.

The decrease in phagocytic function and recycling of the membrane suggested that particulates may also affect the ability of tissue macrophages to undergo proliferative turnover for replenishment or maintenance[40]. We assessed Ki-67 expression in situ as a marker of proliferating cells (Fig. 4e,f). In LN samples from younger donors (≤39 years), the numbers of proliferating $CD68^+CD169^-$ and $CD68^+CD169^+$ macrophages were greater than the number of proliferating $CD68^-CD169^+$ macrophages. In contrast, $CD68^+CD169^-$ macrophages from older donors (≥65 years) had significantly decreased proliferation independent of particulate content (Fig. 4f). $CD68^+CD169^-$ macrophages with or without particulates did not show a direct correlation in Ki67 expression (Extended Data Fig. 5b). The decreased proliferation of $CD68^+CD169^-$ macrophage subsets in older individuals (independent of particulates) suggests that particulates do not affect turnover, but rather decreased turnover is a potential mechanism for the accumulation of particulates within macrophages at older ages.

### Particulates alter cytokine production by macrophages

Macrophages also elicit critical innate immune functions through the secretion of multiple proinflammatory and regulatory cytokines and mediators[41]. To define how particulate content affects macrophage-derived cytokine production, we stained LLN sections with antibodies to macrophage-derived factors including the antiviral cytokine interferon-α (IFN-α), the proinflammatory cytokines tumor necrosis factor-α (TNF-α) and interleukin-6 (IL-6) and the anti-inflammatory mediator arginase[42]. We previously found that human LLNs exhibit ongoing immune activity compared with other LN sites[23], enabling in situ examination of cytokine production. To dissect the individual contributions of particulates and age in macrophage function, we measured cytokine production by $CD68^+CD169^-$ macrophages with and without particulates in LLNs across all adult ages (Fig. 5 and Extended Data Fig. 6). For each parameter measured, we performed a multivariable regression analysis to control for particulate and age effects (Supplementary Table 1).

Across ages, macrophages containing particulates exhibited decreased frequencies of cytokine production compared with macrophages without particulates for IFN-α, TNF-α and IL-6 (Fig. 5a–f, Extended Data Fig. 6a–c and Supplementary Table 1). This finding is consistent with particulates having inhibitory effects on macrophage function. In contrast, arginase was produced comparably by macrophages containing or lacking particulates (Extended Data Fig. 6d–f). When comparing functional capacity across age, we found three patterns showing differential effects of particulates and age for various mediators. For TNF-α, there was an age-associated increase in the frequency of TNF-$\alpha^+$ macrophages independent of particulates, although

**Fig. 5 | Particulate-containing $CD68^+CD169^-$ macrophages exhibit altered cytokine production. a**, Confocal images of human LLNs stained for CD68, CD169 and TNF-α from donors of the indicated ages. The arrows show representative $CD68^+CD169^-$ macrophages (magenta, $CD68^+CD169^-$ macrophages with particulates; orange, $CD68^+CD169^-$ macrophages without particulates). The left column shows brightfield imaging overlays (particulates are white). Representative images were taken from 2–5 donors (3–4 images per donor) per age group (≤39, 40–64 and ≥65 years). Scale bars, 20 µm. **b**, Graph showing the paired frequencies of TNF-$\alpha^+$ $CD68^+CD169^-$ macrophages with or without black particulates, as calculated using Imaris software. Statistical significance was assessed using repeated measures ANOVA. Statistically significant differences were found for the following comparisons of with versus without particulates: $P = 0.0021$(**) for ≤39 years, $P = 0.0018$(**) for 40–64 years and $P = 0.0092$(**) for ≥65 years. The data are from ten donors (3–4 single images per donor). **c**, Graphs showing the frequencies of TNF-$\alpha^+$ $CD68^+CD169^-$ macrophages with or without particulates by age, as calculated using Imaris software ($n = 10$). Linear regression was performed with Pearson's correlation (two tailed). *P* values and Pearson's *R* values are provided (*, $p<0.05$). The data are presented as means ± 95% CIs. **d**, As in **a**, but with staining for IFN-α instead of TNF-α. Representative images were taken from 4–6 donors (2–4 images per donor) per age group (≤39, 40–64 and ≥65 years). Scale bars, 20 µm. **e**, As in **b**, but for IFN-$\alpha^+$ $CD68^+CD169^-$ macrophages. The *P* values for comparisons of with versus without black particulates were $P = 0.0021$(**) for ≤39 years, $P = 0.0036$(**) for 40–64 years and $P = 0.4170$(n.s.) for ≥65 years. The data are from 15 donors (2–4 single images per donor). **f**, As in **c**, but for IFN-$\alpha^+$ $CD68^+CD169^-$ macrophages ($n = 15$). (**, $p < 0.01$).

https://doi.org/10.1038/s41591-022-02073-x

the frequency of TNF-α$^+$ macrophages with particulates was lower at all ages (Fig. 5a–c). Multivariate analysis showed significant yet independent effects of particulates and age for TNF-α (Supplementary Table 1). For IFN-α expression, we found a significant increase with age only in the particulate-containing macrophage subset, and multivariate analysis further revealed independent effects of particulates, with decreased

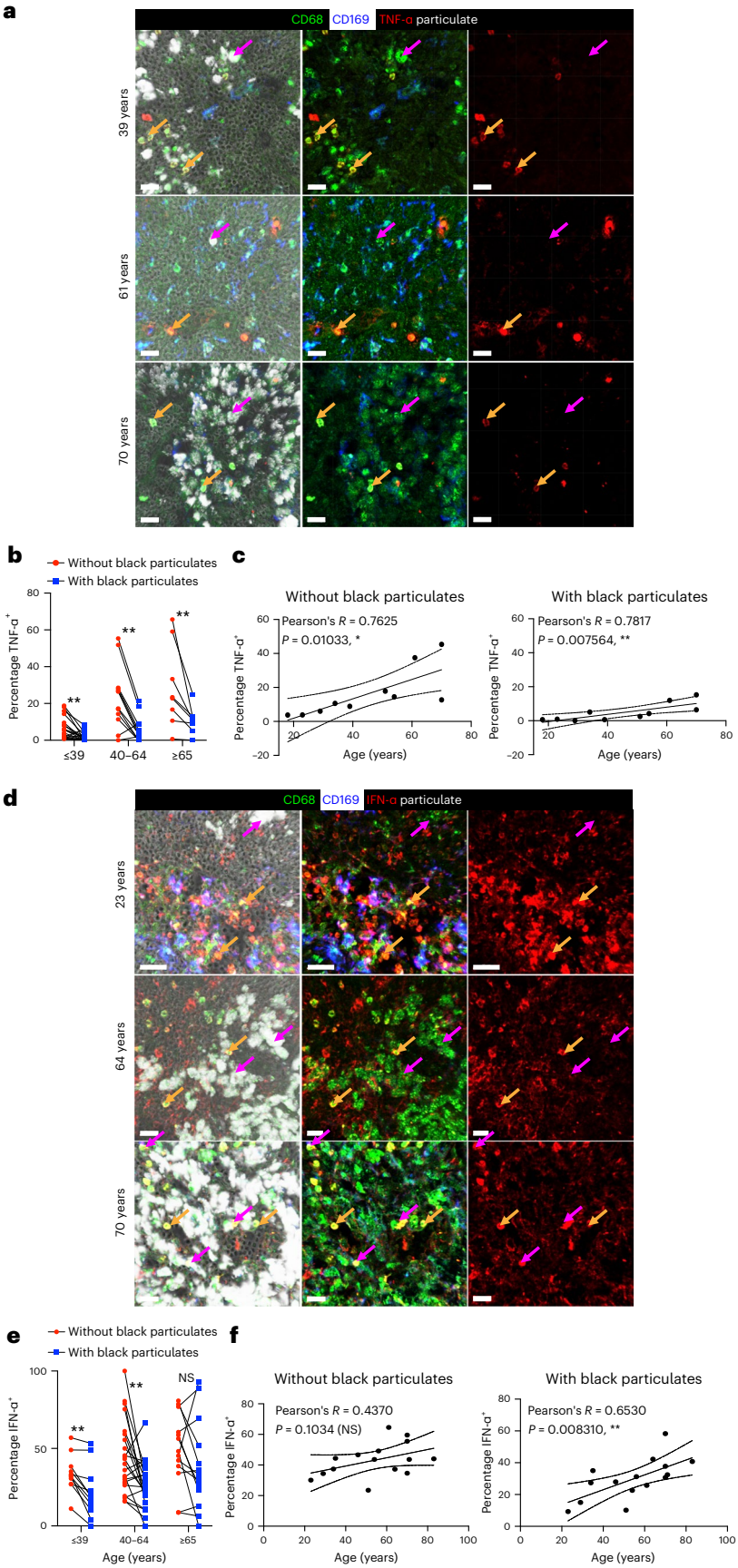

https://doi.org/10.1038/s41591-022-02073-x

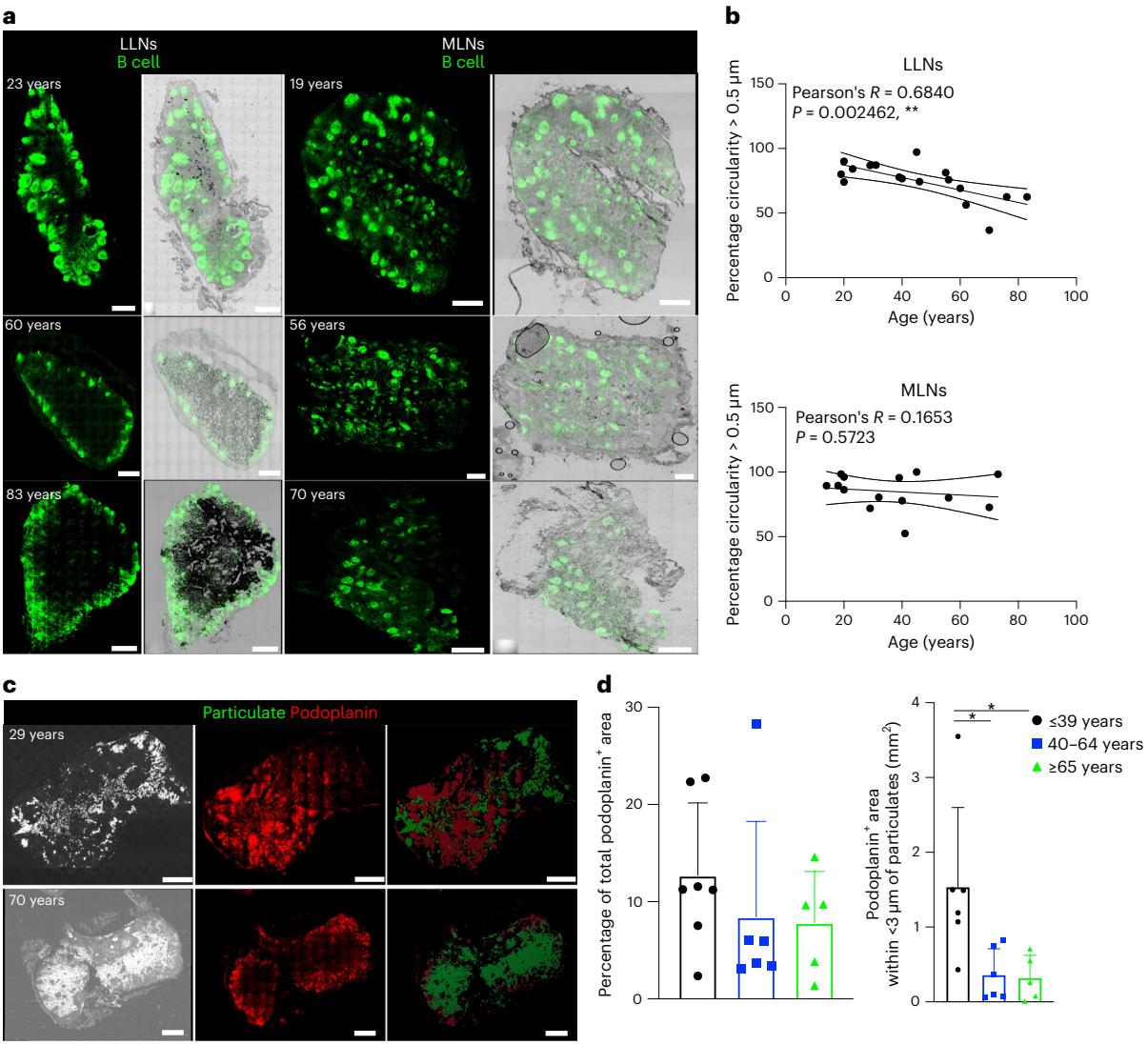


**Fig. 6 | Disrupted LN architecture in the presence of particulate matter.** **a**, Representative confocal images of whole human LN sections from donors of the indicated ages, stained for CD20 to show B cell follicles (green) and with brightfield imaging overlays (white) to show black particulate matter. Representative images were taken from 3–7 donors (LLNs) and 2–8 donors (MLNs) per age group (≤39, 40–64 and ≥65 years). Scale bars, 1,000 µm. **b**, B cell circularity measured using an open-source code (see Methods) to quantify B cell follicle integrity in MLNs ($n = 14$) and LLNs ($n = 17$). The graphs show the circularity measurement above a threshold (>0.5 µm) for each whole LN section obtained from organ donors of the indicated ages. Linear regression was performed with Pearson's correlation (two tailed). *P* values and Pearson's *R* values are provided (** for p<0.01). The data are presented as means ± 95% CIs. **c**, Representative confocal images of human LLNs (from donors of the indicated ages) stained for podoplanin to show the lymphatics (red; middle). Brightfield imaging overlays (white; left) show the black particulate matter. In the right column, they are pseudocolored green to show the overlay with podoplanin (the particulate matter and lymphatics were isosurfaced using Imaris software). Representative images were taken from 5–12 donors per age group (≤65 and ≥65 years). Scale bars, 1,000 µm. **d**, Left, graph showing the percentage of the whole LN section covered by lymphatics. Right, graph showing the area covered by lymphatics close to the particulate area (<3 µm), as determined using Imaris software. Statistical significance was determined by one-way ANOVA with Tukey's post-hoc test. Statistically significant differences were found for the following comparisons of podoplanin$^+$ area (right graph): ≤39 versus 40–64 years ($P = 0.0257$, *) and ≤39 versus ≥65 years ($P = 0.0279$, *). The data are presented as means ± s.d. and are from 17 donors.

IFN-α expression at younger ages (Fig. 5d–f and Supplementary Table 1). In contrast, both arginase and IL-6 did not show age-associated changes in their expression, although IL-6 expression was decreased in particulate- compared with non-particulate-containing macrophages (Extended Data Fig. 6a–f and Supplementary Table 1). Together, these results show independent and synergistic effects of particulates and age on macrophage function in LLNs.

## Particulates disrupt LN architecture and lymphatic drainage

Adaptive immune responses are primed within LN follicles, where T cells interact with B cells to promote the production of antibody-secreting plasma cells and memory B cells[43]. Disruptions of these follicles due to cytokines, chemokines or infections can lead to a decreased adaptive immune response[44,45]. In addition, structural connections with lymphatic vessels are important for the transit of immune cells throughout tissues and for migration of dendritic cells from tissues to LNs for T cell priming[46]. We investigated whether the accumulation of carbon particulates in aging LLNs affects LN architecture and immunosurveillance. We observed that B cell follicles in LLNs became more dispersed with age, resulting in a loss of B cell follicle integrity, as quantified using a computational measure of follicle circularity, while follicles within MLNs did not exhibit significant structural changes with age (Fig. 6a,b).

Similarly, an assessment of lymphatics by staining human LN sections with podoplanin[47] (Fig. 6c) revealed a slight decrease in the total lymphatics area in both LLNs and MLNs with age, but this did not achieve significance (Fig. 6d). However, in regions containing particulate matter, there were significantly fewer lymphatic vessels in older compared with younger adults (Fig. 6d). The accumulation of carbon particulates is therefore accompanied by a disruption in LN architecture, affecting follicles and lymphatic drainage, with potential impacts on the priming of adaptive immunity and immune surveillance.

## Discussion

Diseases of the lungs and respiratory tract disproportionately affect older people, as evidenced by the dramatically increased susceptibility to respiratory infections that has been observed during the SARS-CoV-2 pandemic. Here, we reveal a new mechanism for compromised respiratory immunity with increasing age due to exposure to inhaled particulates from the environment that have specific effects on LLNs, which provide critical immunosurveillance functions. We show that particulates are contained within TCZMs in LLNs but are not present in TCZMs in MLNs within the same individual. Particulate-containing macrophages exhibit decreased phagocytosis over age, probably due to the direct effects of particulates, which also decreases cytokine production and can exacerbate age-associated inflammation. Moreover, increased particulate content after the age of 40 years results in a disruption of LN structure and lymphatic connections. Our findings provide evidence for individual and cumulative effects of environmental insults and senescent changes on lung-localized immunity.

Macrophages orchestrate the innate immune response through their phagocytic uptake of pathogens and the production of cytokines for immune cell recruitment and the initiation of adaptive immunity. They also maintain tissue homeostasis through the uptake and elimination of dead cells and debris[48,49]. Here, we provide direct evidence that macrophages take up atmospheric particulates that lodge in LLNs. Whether these macrophages originate in the lungs is not known, although the increased prevalence of $CD68^{+}CD169^{-}$ macrophages in LLNs versus MLNs suggests recruitment to LLNs from the lungs. Our results also indicate that the fate of particulate-containing macrophages may differ with age. Macrophages in the LNs of younger individuals exhibited higher turnover than those from older individuals, which may facilitate particulate clearance. In this way, young macrophages may be more resilient to the detrimental effects of particulate accumulation.

Particulates also have adverse effects on macrophage function. We showed that a high concentration of particulates can be engulfed by macrophages, which results in impaired phagocytic capacity mediated by direct recognition via scavenger receptors or other non-opsonized pathways. Whether phagocytosis of pathogens and cellular debris or Fc receptor-mediated opsonization are affected remains to be established. We also detected independent effects of particulates on cytokine production by macrophages. Particulate-containing macrophages exhibited lower production of key proinflammatory cytokines including TNF-α, IFN-α and IL-6, which are essential for innate responses to pathogens. We therefore propose a direct effect of particulates in multiple aspects of macrophage function and turnover. The resultant persistence of functionally impaired macrophages in LLNs may contribute to the dysregulated innate responses to respiratory pathogens known to occur in older people[5,50].

We also found disrupted follicular structure and decreased lymphatic connections in LLNs with high particulate content, mostly found in individuals older than 50 years. These results suggest impaired priming of adaptive immune responses for newly encountered respiratory pathogens, which is known to occur with age[5]. However, the ability of particulate-containing LNs to support priming needs to be specifically investigated. Older individuals are intrinsically compromised in their ability to respond to new pathogens due to diminished numbers of naive T cells and a lack of thymic output[51]. The loss of structural niches for priming in LLNs further exacerbates the impact of these senescent changes on respiratory immunity. In our previous studies, we showed that the proportions of tissue-resident memory T cells and influenza virus-specific tissue-resident memory T cells were maintained over age in human lungs, but decreased in frequency in LLNs[24,52,53], suggesting that altered LLN architecture also impacts the maintenance of memory T cells. Together, our findings indicate that age-associated changes to the immune system are local and anatomical, as well as intrinsic to specific cell types.

Pollution from carbon-based sources is an ongoing and growing threat to the health and livelihood of the world's population[54]. The specific effects of pollutants on lung inflammation and asthma in certain individuals or within certain geographic regions have been documented[55–57]. Here, through examination of lymphoid tissues, we demonstrate a chronic and ubiquitous impact of pollution on our ability to mount critical immune defense and surveillance of the lungs. In this way, older people are highly vulnerable to pathogens that infect the respiratory tract, as has been tragically demonstrated with the COVID-19 pandemic. The effects of pollutants on neurodegenerative disease are also well documented[58,59] and neuroinflammation is implicated in this process[60]. We therefore propose that policies to limit carbon emissions will not only improve the global climate, but also preserve our immune systems and their ability to protect against current and emerging pathogens and to maintain tissue health and integrity.

In conclusion, our results provide direct evidence that the environment can have cumulative and adverse effects on our immune system with age. We show how environmental pollutants specifically target immune cells within lymphoid organs, which carry out essential immune surveillance functions. These findings can inform how we monitor and study our immune system—in health and disease and with age.

## Online content

Any methods, additional references, Nature Research reporting summaries, source data, extended data, supplementary information, acknowledgements, peer review information; details of author contributions and competing interests; and statements of data and code availability are available at https://doi.org/10.1038/s41591-022-02073-x.

## References

1. Schneider, J. L. et al. The aging lung: physiology, disease, and immunity. *Cell* **184**, 1990–2019 (2021).
2. *Why Population Aging Matters: A Global Perspective* (National Institute on Aging et al., 2007).
3. Pop-Vicas, A. & Gravenstein, S. Influenza in the elderly: a mini-review. *Gerontology* **57**, 397–404 (2011).
4. O'Driscoll, M. et al. Age-specific mortality and immunity patterns of SARS-CoV-2. *Nature* **590**, 140–145 (2021).
5. Akbar, A. N. & Gilroy, D. W. Aging immunity may exacerbate COVID-19. *Science* **369**, 256–257 (2020).
6. Metcalf, C. J. E. et al. Comparing the age and sex trajectories of SARS-CoV-2 morbidity and mortality with other respiratory pathogens. *R. Soc. Open Sci.* **9**, 211498 (2022).
7. Presley, C. J., Reynolds, C. H. & Langer, C. J. Caring for the older population with advanced lung cancer. *Am. Soc. Clin. Oncol. Educ. Book* **37**, 587–596 (2017).
8. Lopez-Otin, C., Blasco, M. A., Partridge, L., Serrano, M. & Kroemer, G. The hallmarks of aging. *Cell* **153**, 1194–1217 (2013).
9. Frasca, D. & Blomberg, B. B. Inflammaging decreases adaptive and innate immune responses in mice and humans. *Biogerontology* **17**, 7–19 (2016).
10. Williams, A. E., Jose, R. J., Brown, J. S. & Chambers, R. C. Enhanced inflammation in aged mice following infection with *Streptococcus pneumoniae* is associated with decreased IL-10 and augmented chemokine production. *Am. J. Physiol. Lung Cell. Mol. Physiol.* **308**, L539–L549 (2015).

11. Nilsson Sommar, J. et al. Long-term exposure to particulate air pollution and black carbon in relation to natural and cause-specific mortality: a multicohort study in Sweden. *BMJ Open* **11**, e046040 (2021).
12. Weisberg, S. P., Ural, B. B. & Farber, D. L. Tissue-specific immunity for a changing world. *Cell* **184**, 1517–1529 (2021).
13. Legge, K. L. & Braciale, T. J. Lymph node dendritic cells control $CD8^+$ T cell responses through regulated FasL expression. *Immunity* **23**, 649–659 (2005).
14. Paik, D. H. & Farber, D. L. Influenza infection fortifies local lymph nodes to promote lung-resident heterosubtypic immunity. *J. Exp. Med.* **218**, e20200218 (2021).
15. Masters, A. R. et al. Assessment of lymph node stromal cells as an underlying factor in age-related immune impairment. *J. Gerontol. A Biol. Sci. Med. Sci.* **74**, 1734–1743 (2019).
16. Luscieti, P., Hubschmid, T., Cottier, H., Hess, M. W. & Sobin, L. H. Human lymph node morphology as a function of age and site. *J. Clin. Pathol.* **33**, 454–461 (1980).
17. Hadamitzky, C. et al. Age-dependent histoarchitectural changes in human lymph nodes: an underestimated process with clinical relevance? *J. Anat.* **216**, 556–562 (2010).
18. Buettner, M. & Bode, U. Lymph node dissection—understanding the immunological function of lymph nodes. *Clin. Exp. Immunol.* **169**, 205–212 (2012).
19. Davies, M. L. et al. A systemic macrophage response is required to contain a peripheral poxvirus infection. *PLoS Pathog.* **13**, e1006435 (2017).
20. Farber, D. L. Tissues, not blood, are where immune cells act. *Nature* **593**, 506–509 (2021).
21. Carpenter, D. J. et al. Human immunology studies using organ donors: impact of clinical variations on immune parameters in tissues and circulation. *Am. J. Transpl.* **18**, 74–88 (2018).
22. Dogra, P. et al. Tissue determinants of human NK cell development, function, and residence. *Cell* **180**, 749–763 (2020).
23. Granot, T. et al. Dendritic cells display subset and tissue-specific maturation dynamics over human life. *Immunity* **46**, 504–515 (2017).
24. Thome, J. J. et al. Spatial map of human T cell compartmentalization and maintenance over decades of life. *Cell* **159**, 814–828 (2014).
25. Miron, M. et al. Human lymph nodes maintain TCF-$1^{hi}$ memory T cells with high functional potential and clonal diversity throughout life. *J. Immunol.* **201**, 2132–2140 (2018).
26. Schantz, M. M. et al. Development of two fine particulate matter standard reference materials (<4 µm and <10 µm) for the determination of organic and inorganic constituents. *Anal. Bioanal. Chem.* **408**, 4257–4266 (2016).
27. Bellomo, A., Gentek, R., Bajenoff, M. & Baratin, M. Lymph node macrophages: scavengers, immune sentinels and trophic effectors. *Cell Immunol.* **330**, 168–174 (2018).
28. Gray, E. E. & Cyster, J. G. Lymph node macrophages. *J. Innate Immun.* **4**, 424–436 (2012).
29. Davies, L. C., Jenkins, S. J., Allen, J. E. & Taylor, P. R. Tissue-resident macrophages. *Nat. Immunol.* **14**, 986–995 (2013).
30. Ural, B. B. et al. Identification of a nerve-associated, lung-resident interstitial macrophage subset with distinct localization and immunoregulatory properties. *Sci. Immunol.* **5**, eaax8756 (2020).
31. O'Neill, A. S., van den Berg, T. K. & Mullen, G. E. Sialoadhesin—a macrophage-restricted marker of immunoregulation and inflammation. *Immunology* **138**, 198–207 (2013).
32. Martinez-Pomares, L. & Gordon, S. $CD169^+$ macrophages at the crossroads of antigen presentation. *Trends Immunol.* **33**, 66–70 (2012).
33. Baratin, M. et al. T cell zone resident macrophages silently dispose of apoptotic cells in the lymph node. *Immunity* **47**, 349–362 (2017).
34. Tremble, L. F. et al. Differential association of $CD68^+$ and $CD163^+$ macrophages with macrophage enzymes, whole tumour gene expression and overall survival in advanced melanoma. *Br. J. Cancer* **123**, 1553–1561 (2020).
35. Etzerodt, A. & Moestrup, S. K. CD163 and inflammation: biological, diagnostic, and therapeutic aspects. *Antioxid. Redox Signal.* **18**, 2352–2363 (2013).
36. Medina-Contreras, O. et al. CX3CR1 regulates intestinal macrophage homeostasis, bacterial translocation, and colitogenic Th17 responses in mice. *J. Clin. Invest.* **121**, 4787–4795 (2011).
37. Ensan, S. et al. Self-renewing resident arterial macrophages arise from embryonic $CX3CR1^+$ precursors and circulating monocytes immediately after birth. *Nat. Immunol.* **17**, 159–168 (2016).
38. Erdman, L. K. et al. CD36 and TLR interactions in inflammation and phagocytosis: implications for malaria. *J. Immunol.* **183**, 6452–6459 (2009).
39. Schulz, D., Severin, Y., Zanotelli, V. R. T. & Bodenmiller, B. In-depth characterization of monocyte-derived macrophages using a mass cytometry-based phagocytosis assay. *Sci. Rep.* **9**, 1925 (2019).
40. Hashimoto, D. et al. Tissue-resident macrophages self-maintain locally throughout adult life with minimal contribution from circulating monocytes. *Immunity* **38**, 792–804 (2013).
41. Cox, N., Pokrovskii, M., Vicario, R. & Geissmann, F. Origins, biology, and diseases of tissue macrophages. *Annu. Rev. Immunol.* **39**, 313–344 (2021).
42. Sica, A. & Mantovani, A. Macrophage plasticity and polarization: in vivo veritas. *J. Clin. Invest.* **122**, 787–795 (2012).
43. Huang, Q., Xu, L. & Ye, L. T cell immune response within B-cell follicles. *Adv. Immunol.* **144**, 155–171 (2019).
44. Popescu, M., Cabrera-Martinez, B. & Winslow, G. M. TNF-α contributes to lymphoid tissue disorganization and germinal center B cell suppression during intracellular bacterial infection. *J. Immunol.* **203**, 2415–2424 (2019).
45. Kaneko, N. et al. Loss of Bcl-6-expressing T follicular helper cells and germinal centers in COVID-19. *Cell* **183**, 143–157 (2020).
46. Petrova, T. V. & Koh, G. Y. Biological functions of lymphatic vessels. *Science* **369**, eaax4063 (2020).
47. Schacht, V. et al. T1α/podoplanin deficiency disrupts normal lymphatic vasculature formation and causes lymphedema. *EMBO J.* **22**, 3546–3556 (2003).
48. Arandjelovic, S. & Ravichandran, K. S. Phagocytosis of apoptotic cells in homeostasis. *Nat. Immunol.* **16**, 907–917 (2015).
49. Kurosaka, K., Takahashi, M., Watanabe, N. & Kobayashi, Y. Silent cleanup of very early apoptotic cells by macrophages. *J. Immunol.* **171**, 4672–4679 (2003).
50. Boe, D. M., Boule, L. A. & Kovacs, E. J. Innate immune responses in the ageing lung. *Clin. Exp. Immunol.* **187**, 16–25 (2017).
51. Nikolich-Zugich, J. Aging of the T cell compartment in mice and humans: from no naive expectations to foggy memories. *J. Immunol.* **193**, 2622–2629 (2014).
52. Kumar, B. V., Connors, T. J. & Farber, D. L. Human T cell development, localization, and function throughout life. *Immunity* **48**, 202–213 (2018).
53. Poon, M. M. L. et al. Heterogeneity of human anti-viral immunity shaped by virus, tissue, age, and sex. *Cell Rep.* **37**, 110071 (2021).
54. Cohen, A. J. et al. Estimates and 25-year trends of the global burden of disease attributable to ambient air pollution: an analysis of data from the Global Burden of Diseases Study 2015. *Lancet* **389**, 1907–1918 (2017).
55. Matthews, N. C. et al. Urban particulate matter-activated human dendritic cells induce the expansion of potent inflammatory Th1, Th2, and Th17 effector cells. *Am. J. Respir. Cell Mol. Biol.* **54**, 250–262 (2016).

56. Brandt, E. B. et al. Exposure to allergen and diesel exhaust particles potentiates secondary allergen-specific memory responses, promoting asthma susceptibility. *J. Allergy Clin. Immunol.* **136**, 295–303 (2015).
57. Guarnieri, M. & Balmes, J. R. Outdoor air pollution and asthma. *Lancet* **383**, 1581–1592 (2014).
58. Haghani, A., Morgan, T. E., Forman, H. J. & Finch, C. E. Air pollution neurotoxicity in the adult brain: emerging concepts from experimental findings. *J. Alzheimers Dis.* **76**, 773–797 (2020).
59. Haghani, A., Thorwald, M., Morgan, T. E. & Finch, C. E. The APOE gene cluster responds to air pollution factors in mice with coordinated expression of genes that differs by age in humans. *Alzheimers Dement.* **17**, 175–190 (2021).
60. Scieszka, D. et al. Neuroinflammatory and neurometabolomic consequences from inhaled wildfire smoke-derived particulate matter in the Western United States. *Toxicol. Sci.* **186**, 149–162 (2022).

# Methods

## Human samples

LN tissues were obtained from brain-dead organ donors through an approved protocol and material transfer agreement with LiveOnNY, the local organ procurement organization for the New York metropolitan area, as previously described[21,24]. Tissues for this study were obtained from donors with no history of asthma and who were negative for SARS-CoV-2, cancer, hepatitis B and C and human immunodeficiency virus. We also selected for donors who were indicated in the donor information sheet as being non-smokers and/or with no history of heavy smoking (>20 packs for >1 year or more) where indicated (82/84 donors). A list of the donors used in this study, along with information on their age and sex, is provided in Extended Data Table 1. This study does not qualify as having performed research on human participants because the tissues were obtained from deceased (brain-dead) organ donors, as confirmed by the Institutional review board at Columbia University.

## Preparation of cell suspensions from tissue samples

Following procurement, organs were transported to the laboratory and maintained in cold media supplemented with 5% fetal bovine serum (FBS) and penicillin/streptomycin with glutamine. LN tissues were dissected out from the lungs or intestines, cleaned of fat and connective tissue, chopped into pieces and incubated with RPMI media (Thermo Fisher Scientific) containing collagenase D (Sigma–Aldrich) and DNase (Sigma–Aldrich) for 60 min at 37 °C. Cells were isolated with additional mechanical digestion and density gradient centrifugation, with high yields of live cells, as previously described[23,25].

## Tissue preparation for confocal imaging

Dissected LN tissues were fixed in paraformaldehyde, lysine and periodate buffer (PLP; 0.05 M phosphate buffer, 0.1 M L-lysine (pH 7.4), 2 mg ml$^{-1}$ $NaIO_4$ and 10 mg ml$^{-1}$ paraformaldehyde) overnight at 4 °C (Supplementary Table 3). The following day, tissues were dehydrated in 30% sucrose overnight at 4 °C and subsequently embedded in Optimal Cutting Temperature compound. Donor LNs bearing identification numbers of <410 were fixed in phosphate-buffered saline (PBS) solution with 1% paraformaldehyde and 0.1 M L-lysine, incubated in 20% sucrose at 4 °C and subsequently embedded in Optimal Cutting Temperature compound. Frozen tissues were sectioned using a Leica 3050 S cryostat at 20 µm thickness. Intracellular staining media was prepared with PBS containing 2% goat serum, 2% FBS, 0.05% Tween-20 and 0.3% Triton-X. Tissues were blocked with Human TruStain FcX (BioLegend; 1:100 dilution) in intracellular staining media for 1 h at room temperature. Sections were washed with the intracellular staining buffer and stained with the indicated antibodies (Supplementary Table 2) at 1:25 dilution for 1 h at room temperature. Cytokine staining was performed with their corresponding isotypes to eliminate any signal due to non-specific binding. Images were acquired with a Nikon Eclipse Ti inverted confocal microscope using the dry 20× objective. For fluorescence detection, the following lasers were used: 405, 488,561 and 638 nm. For imaging of whole LN sections, 70–400 20× images were acquired depending on the size of the LN, then computationally stitched using NIS-Elements software (Nikon). Single 20× images were imaged in 2 µm 3× Z-steps. Images were analyzed using Imaris software (Bitplane, Oxford Instruments; version 9.5/9.6), including spot, surface, shortest distance, circularity, isosurfacing and pseudocoloring functions.

## Flow cytometry

LN cells were enriched for $CD3^-$ cells using biotin-conjugated anti-CD3 and an EasySep Human Biotin Positive Selection Kit II (STEMCELL Technologies; Supplementary Table 3). Following enrichment, LN cells were resuspended in FACS buffer (PBS, 5% FBS and 0.5% sodium azide) and stained for surface markers at a 1:100 dilution for 20 min at 4 °C (Supplementary Table 2). For intracellular staining, cells were resuspended with Fixation/Permeabilization Concentrate and incubated for 60 min at room temperature as indicated in the Tonbo Biosciences Transcription Factor Staining Buffer Kit (TNB-0607-KIT). Cells were washed with permeabilization buffer, resuspended in the permeabilization buffer with antibodies at a 1:100 dilution and incubated for 60 min at room temperature. Cells were then washed and resuspended in FACS buffer, then analyzed by flow cytometry using a BD LSR II cytometer (Becton Dickinson) and the data were analyzed using FlowJo software (Tree Star version 10.7.1). To generate the heat map of marker expression, geometric mean fluorescence intensities for each surface marker were exported from FlowJo, normalized to the average expression of each marker across the subsets and plotted in Python using the seaborn package.

## Phagocytosis assay

The human macrophage line THP-1 (kindly provided by S. Ghosh) was maintained in RPMI 1640 medium supplemented with 10% FBS and 10,000 IU penicillin (per ml), 10,000 µg ml$^{-1}$ streptomycin and 29.2 mg ml$^{-1}$ L-glutamine (Thermo Fisher Scientific). THP-1 cells ($4 \times 10^4$) were differentiated using (400 nM) Phorbol 12-myristate 13-acetate (Sigma–Aldrich) for 3 d in 6-well plates and the cells were rested overnight in fresh media (RPMI 1640 medium supplemented with 10% FBS and 10,000 IU penicillin (per ml), 10,000 µg ml$^{-1}$ streptomycin and 29.2 mg ml$^{-1}$ L-glutamine). Atmospheric particulates purified from air filters and analyzed by the National Institute of Standards and Technology[26] were purchased from Sigma–Aldrich. To test the uptake of particulates, differentiated THP-1 cells were incubated in fresh media with black particulates (0.0006 g ml$^{-1}$) for 6 h at 37 °C. Following incubation, cells were washed twice to remove all of the free-floating particulates and were rested overnight in fresh media. To assess phagocytosis, differentiated THP-1 cells without particulates (control) and with particulates were cultured in live imaging solution with pHrodo Red *E. coli* BioParticles, according to the manufacturer's protocol, at 4 °C (control condition) or 37 °C (experimental condition) for 90 min. Fresh live imaging solution was added to the cells and they were imaged immediately using confocal microscopy.

## Statistical analysis

Statistical analysis was performed using Prism 8.2.0 (GraphPad) with the exception of the multivariable regression analysis, which was done using Excel version 16.54. For correlations with age, Pearson's correlation was used, and Pearson's $R$ values and their associated $P$ values are included in the figures. Statistical comparisons between two groups were performed using a Student's $t$-test. To assess differences between cytokine production and Ki-67 in macrophages with and without particulates, we used repeated measures two-way analysis of variance (ANOVA). To further assess the differences in cytokine production, multivariable regression analysis was used to control for particulate- and age-related effects. Where noted, three or more groups were analyzed using one-way ANOVA, two-way ANOVA or mixed-effects analysis with Tukey's post-hoc test. As indicated in the captions, the use of asterisks to indicate significance as determined in Prisms was as follows: ns: $p>0.05$; * $p<0.05$; ** $p<0.01$; *** $p<0.001$; **** $p<0.0001$.

## Reporting summary

Further information on research design is available in the Nature Research Reporting Summary linked to this article.

# Data availability

Source data are provided with this paper.

# Code availability

The Python code used to analyze B cell circularity is available from GitHub (https://github.com/Ironhorse1618/Python3.7-Imaris-XTensions).

## Acknowledgements
This work was supported by National Institutes of Health (NIH) grants HL145547, AI106697 and AI128949 awarded to D.L.F. B.B.U. was supported by NIH T32HL105323. P.D. was supported by a Cancer Research Institute Irvington Postdoctoral Fellowship. N.L. is supported by the National Science Foundation Graduate Research Fellowship Program. P.A.S. is supported by the Canadian Institutes of Health Research Fellowship. This study also used the Confocal and Specialized Microscopy Shared Resource core supported by NIH P30 CA013696 and the Columbia Center for Translational Immunology Flow Cytometry Core supported in part by NIH S10RR027050. We thank M. J. Gastinger (Imaris) for the Python code used in the B cell imaging analysis, A. Urso for previous help with confocal microscopy, S. Ghosh for the THP-1 cell line, and the transplant coordinators at LiveOnNY and the donor families for making this study possible.

## Author contributions
B.B.U. designed the experiments, processed the tissues, performed the imaging and flow cytometry, analyzed the data, produced the figures and wrote the paper. P.D., S.B.W., D.P.C. and P.A.S. helped with data analysis and visualization. T.G. made the initial observations of LN particulates and generated the whole-tissue photos. T.S. prepared the tissue samples. P.D., S.B.W., D.P.C., P.A.S., M.M.L.P., N.L., P.T. and Y.S.L. assisted with the tissue processing. T.S., M.K. and R.M. obtained the donor tissues. D.L.F. planned the experiments, coordinated the tissue acquisition and data acquisition/analysis, analyzed the data and wrote and edited the paper.

## Competing interests
The authors declare no competing interests.

## Additional information
**Extended data** is available for this paper at https://doi.org/10.1038/s41591-022-02073-x.

**Supplementary information** The online version contains supplementary material available at https://doi.org/10.1038/s41591-022-02073-x.

**Correspondence and requests for materials** should be addressed to Donna L. Farber.

**Peer review information** *Nature Medicine* thanks the anonymous reviewers for their contribution to the peer review of this work. Primary Handling Editors: Saheli Sadanand and Joao Monteiro, in collaboration with the *Nature Medicine* team.

https://doi.org/10.1038/s41591-022-02073-x

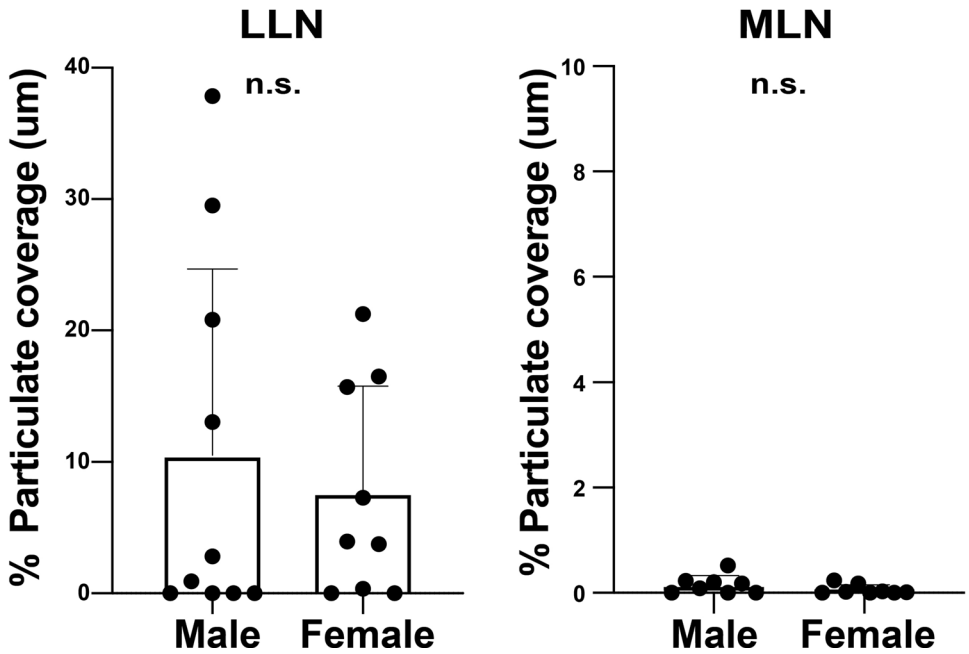


**Extended Data Fig. 1 | Carbon particulate content in different lymph nodes is similar between males and females.** Carbon particulate content in the lung-associated lymph node (LLN) and mesenteric lymph node (MLN) of donors from Fig. 1 stratified by sex. Data from 16–19 donors per site. Significance calculated by student T-test (two-tailed). Data presented as the mean ± SEM. N.S.: not significant by student's t-test.

https://doi.org/10.1038/s41591-022-02073-x

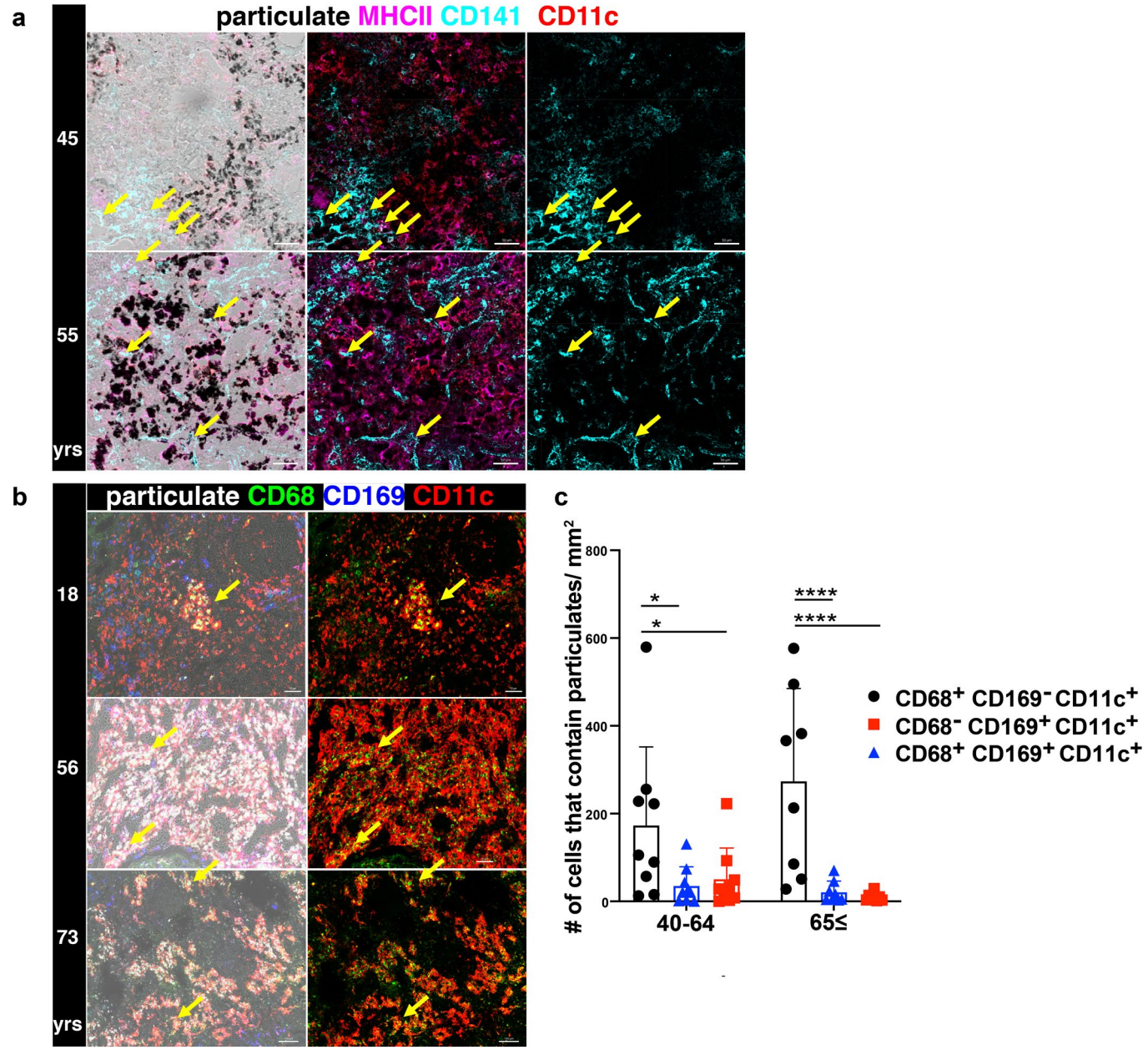


**Extended Data Fig. 2 | Particulate uptake occurs within CD11c+ macrophages but not dendritic cells (DC). a.** Confocal image of human LLNs stained for MHCII (HLA-DR), CD11c, and CD141 expression to identify DC ($CD11c^+HLA\text{-}DR^+CD141^+$) shown with overlay of brightfield (left columns) for visualizing particulates (middle and right columns). Representative images were taken from 5 donors. Scale bar: 50 um. **b.** Confocal image of human LLNs stained for macrophage markers CD68 and CD169 along with CD11c. The image on the left show with overlay of brightfield (left columns) to show localization of particulates (white). The image on the right shows the CD68 and CD11c expression on macrophages. Representative images were taken from 6–9 donors per age group (≤39,40–64 and ≥65 yrs). Scale bar: 50–100 um. **c.** Graphs shows particulate content in specific macrophage subsets for different age groups, quantitated using Imaris software. Significance calculated by 2-way ANOVA with Tukey's posttest, $^*P < 0.05$, $^{****}P < 0.0001$. Significance for 40–64: $CD68^+CD169^-CD11c^+$ vs. $CD68^+CD169^+CD11c^+$ P = 0.0144, $CD68^+CD169^-CD11c^+$ vs. $CD68^-CD169^+CD11c^+$ P = 0.0316; 65 ≤ : $CD68^+CD169^-CD11c^+$ vs. $CD68^+CD169^+CD11c^+$ P = < 0.0001, $CD68^+CD169^-CD11c^+$ vs. $CD68^-CD169^+CD11c^+$ P = < 0.0001. Data presented as the mean ± SD. Data are from 17 donors.

https://doi.org/10.1038/s41591-022-02073-x

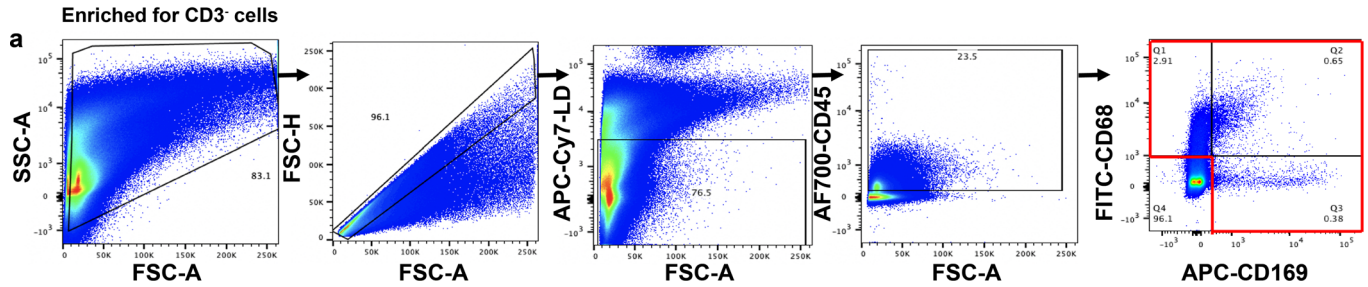


**Extended Data Fig. 3 | Gating strategy.** Flow cytometry gating for CD68$^+$CD169$^-$, CD68$^-$CD169$^+$, and CD68$^+$CD169$^+$ macrophage subsets following gating on live, singlet, and CD45$^+$ cells.

https://doi.org/10.1038/s41591-022-02073-x

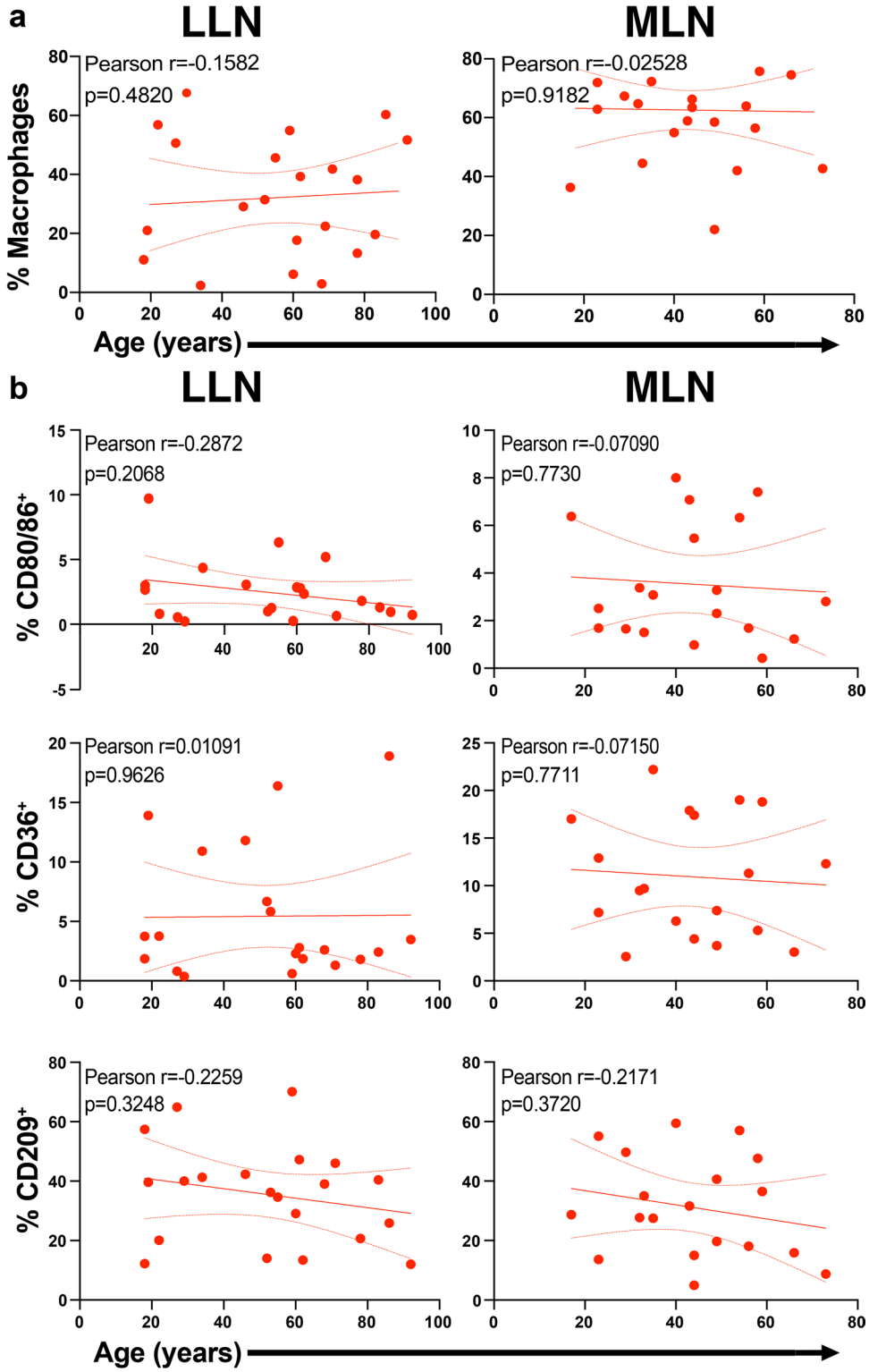


**Extended Data Fig. 4 | CD68−CD169+ macrophages in LN do not exhibit alterations in functional marker expression with age. a.** Frequency of $CD68^{-}CD169^{+}$ macrophages in LLN (n = 21) and MLN (n = 19) over age. Linear regression with Pearson correlation (two-tailed). Pearson r, $^{*}P < 0.033$, $^{**}P < 0.005$ and $^{***}P < 0.001$. Data presented as the mean ± 95% CI. **b.** Expression of functional markers CD80/86, CD36, and CD209 expression on $CD68^{-}CD169^{+}$ macrophages over age by flow cytometric analysis of LLNs (n = 21, left column) and MLNs (n = 19, right column). Linear regression with Pearson correlation (two-tailed). Pearson r, $^{*}P < 0.033$. Data presented as the mean ± 95% CI.

https://doi.org/10.1038/s41591-022-02073-x

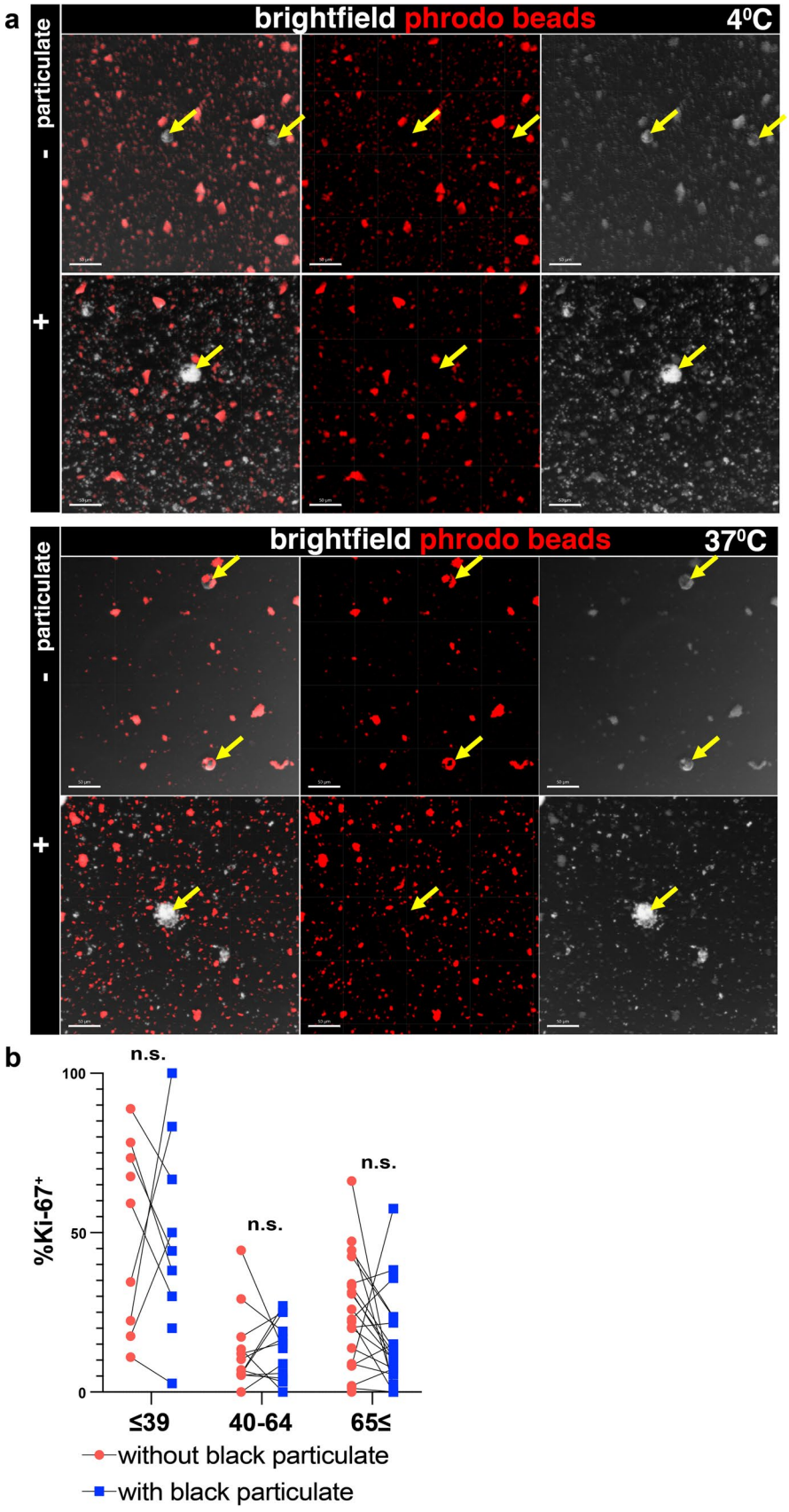


**Extended Data Fig. 5 | See next page for caption.**

https://doi.org/10.1038/s41591-022-02073-x

**Extended Data Fig. 5 | Particulates inhibit phagocytosis but do not alter age-associated effects on proliferation. a**. Particulate containing THP-1 macrophages cannot phagocytose fluorescent pHrodo beads. Representative images of differentiated THP-1 cells previously incubated with (+) or without (-) black particulates subsequently cultured with pHrodo beads at 37 °C or 4 °C for 90 minutes. Confocal image of THP-1 cells imaged for pHrodo beads and brightfield. Yellow arrows indicate THP-1 cells. Scale bar: 50um. Image is representative of two experiments. (n = 9–12 wells/condition). **b**. Imaging data from Fig. 3g analyzed for $Ki67^{+}$ $CD68^{+}CD169^{-}$ macrophages that are within or outside the black particulate area. Significance assessed with paired T-test (two-tailed). Data are from 13 donors (2–7 single images for each donor).

https://doi.org/10.1038/s41591-022-02073-x

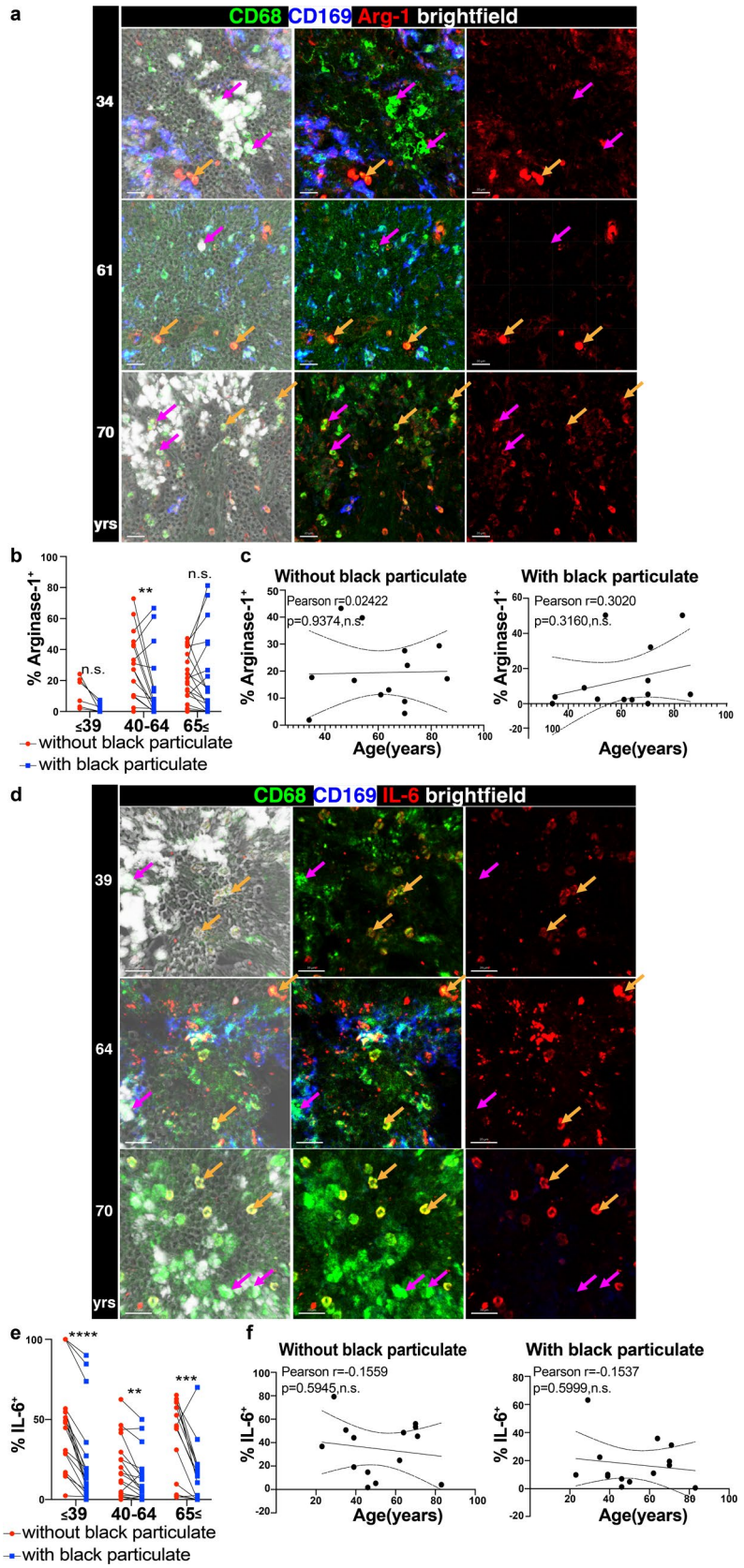


**Extended Data Fig. 6 | See next page for caption.**

https://doi.org/10.1038/s41591-022-02073-x

**Extended Data Fig. 6 | Particulate-containing CD68+CD169− macrophages induce an immunoregulatory environment in the LLNs. a**. Confocal image of human LLNs stained for CD68, CD169, and Arginase-1 from donors of indicated ages. Arrows show representative $CD68^+CD169^-$ macrophages with particulates (magenta) or without particulates (orange). Representative images were taken from 2–6 donors (2–4 images/donor) per age group (≤39,40–64 and ≥65 yrs). Scale bar: 20 um. **b**. Graph shows paired frequencies of $Arg\text{-}1^+CD68^+CD169^-$ macrophages with or without particulates calculated using Imaris software. Significance assessed with repeated measures ANOVA. Significance for ≤39 yrs P = 0.059, 40–64 years P = 0.0088, ≥65 years P = 0.9969. Data are from 13 donors (2–4 single images for each donor). **c**. Graph shows frequency of $Arg\text{-}1^+CD68^+CD169^-$ macrophages with or without particulates over age calculated using Imaris software. (n = 13). Linear regression with Pearson correlation (two-tailed). Pearson r, n.s. Data presented as the mean ± 95% CI. **d**. Confocal image of human LLNs stained for CD68, CD169, and IL-6 from donors of indicated ages. Arrows show representative $CD68^+CD169^-$ macrophages with particulates (magenta) or without particulates (orange). Representative images were taken from 4–5 donors (2–4 images/donor) per age group (≤39,40–64 and ≥65 yrs). Scale bar: 20 um. **e**. Graph shows paired frequencies of $IL\text{-}6^+CD68^+CD169^-$ macrophages with or without particulates calculated using Imaris software. Significance assessed with repeated measures ANOVA. Significance for ≤39 yrs P = < 0.0001, 40–64 years P = 0.0037, ≥65 years P = 0.0002. Data are from 14 donors (2–4 single images for each donor) **f**. Graph shows frequency $IL\text{-}6^+CD68^+CD169^-$ macrophages with or without particulates over age calculated using Imaris software. (n = 14). Linear regression with Pearson correlation (two-tailed). Pearson r, n.s. Data presented as the mean ± 95% CI.

https://doi.org/10.1038/s41591-022-02073-x

**Extended Data Table 1 | Organ donors used in this study**

| Donor # | Age (years) and Sex | Donor # | Age (years) and Sex | Donor # | Age (years) and Sex |
|---|---|---|---|---|---|
| 204 | 30M | 300 | 56M | 433 | 86F |
| 212 | 48 | 307 | 18M | 434 | 46F |
| 217 | 49M | 308 | 68M | 435 | 55F |
| 223 | 29F | 309 | 45F | 436 | 62F |
| 231 | 56M | 314 | 35F | 439 | 62F |
| 236 | 75F | 317 | 23F | 442 | 19M |
| 239 | 93F | 319 | 11M | 444 | 34F |
| 242 | 20F | 321 | 17F | 447 | 40F |
| 245 | 50F | 322 | 32M | 451 | 54F |
| 247 | 45F | 324 | 56M | 454 | 27F |
| 250 | 39F | 329 | 43F | 455 | 70M |
| 252 | 72M | 338 | 49M | 456 | 53M |
| 253 | 23M | 340 | 23M | 459 | 52F |
| 255 | 63F | 341 | 49M | 461 | 22F |
| 256 | 70M | 342 | 59M | 462 | 76F |
| 259 | 46M | 344 | 44M | 465 | 15M |
| 262 | 73M | 345 | 73F | 467 | 58F |
| 267 | 70F | 360 | 16M | 481 | 29M |
| 270 | 23F | 410 | 78F | 482 | 66M |
| 274 | 14M | 417 | 78M | 483 | 33M |
| 275 | 31M | 420 | 34M | 484 | 59M |
| 276 | 41M | 421 | 18F | 491 | 44F |
| 279 | 73F | 422 | 60M | 494 | 51M |
| 285 | 53M | 423 | 83M | 502 | 35F |
| 286 | 46M | 424 | 71F | 504 | 39M |
| 288 | 32M | 427 | 69M | 507 | 29M |
| 290 | 77F | 428 | 61M | 509 | 70M |
| 299 | 20M | 430 | 18M | 528 | 64F |

nature portfolio

Corresponding author(s): Donna L. Farber

Last updated by author(s): Sep 28, 2022

# Reporting Summary

Nature Portfolio wishes to improve the reproducibility of the work that we publish. This form provides structure for consistency and transparency in reporting. For further information on Nature Portfolio policies, see our Editorial Policies and the Editorial Policy Checklist.

## Statistics

For all statistical analyses, confirm that the following items are present in the figure legend, table legend, main text, or Methods section.

| n/a | Confirmed |
|---|---|
| ☐ | ☒ The exact sample size (*n*) for each experimental group/condition, given as a discrete number and unit of measurement |
| ☐ | ☒ A statement on whether measurements were taken from distinct samples or whether the same sample was measured repeatedly |
| ☐ | ☒ The statistical test(s) used AND whether they are one- or two-sided<br>*Only common tests should be described solely by name; describe more complex techniques in the Methods section.* |
| ☐ | ☒ A description of all covariates tested |
| ☐ | ☒ A description of any assumptions or corrections, such as tests of normality and adjustment for multiple comparisons |
| ☐ | ☒ A full description of the statistical parameters including central tendency (e.g. means) or other basic estimates (e.g. regression coefficient) AND variation (e.g. standard deviation) or associated estimates of uncertainty (e.g. confidence intervals) |
| ☐ | ☒ For null hypothesis testing, the test statistic (e.g. *F*, *t*, *r*) with confidence intervals, effect sizes, degrees of freedom and *P* value noted<br>*Give P values as exact values whenever suitable.* |
| ☒ | ☐ For Bayesian analysis, information on the choice of priors and Markov chain Monte Carlo settings |
| ☒ | ☐ For hierarchical and complex designs, identification of the appropriate level for tests and full reporting of outcomes |
| ☐ | ☒ Estimates of effect sizes (e.g. Cohen's *d*, Pearson's *r*), indicating how they were calculated |

*Our web collection on statistics for biologists contains articles on many of the points above.*

## Software and code

Policy information about availability of computer code

| | |
|---|---|
| Data collection | Becton-Dickinson LSRII instrument<br>Nikon A1 Scanning Confocal Microscope |
| Data analysis | Python: version 3.7 Python (2020)/ https://www.python.org/downloads/release/python-370/<br>Anaconda: Anaconda (2020)/ https://www.anaconda.com/products/individual-b<br>Flowjo: version 10.7.1 Tree Star/ https://www.flowjo.com/<br>Imaris: version 9.5/9.6 Bitplane; Oxford Instruments /https://imaris.oxinst.com/<br>Prism: version 8.2.0 GraphPad Software/ https://www.graphpad.com/scientific-software/prism/<br>NIS-elements: Nikon/ https://www.microscope.healthcare.nikon.com/products/software/nis-elements<br>Python code used to analyze B cell circularity will be available at GitHub https://github.com/Ironhorse1618/Python3.7-Imaris-XTensions<br>Excel: version 16.54 Microsoft https://www.microsoft.com/en-us/microsoft-365/excel<br>SeBaView Laxco http://www.laxcoinc.com/download |

For manuscripts utilizing custom algorithms or software that are central to the research but not yet described in published literature, software must be made available to editors and reviewers. We strongly encourage code deposition in a community repository (e.g. GitHub). See the Nature Portfolio guidelines for submitting code & software for further information.

## Data

Policy information about availability of data

All manuscripts must include a data availability statement. This statement should provide the following information, where applicable:

- Accession codes, unique identifiers, or web links for publicly available datasets
- A description of any restrictions on data availability
- For clinical datasets or third party data, please ensure that the statement adheres to our policy

Source data from this study are provided for Figures 1-6 and Extended data 1,2,4-6. Additional supporting data will be available upon request.

# Field-specific reporting

Please select the one below that is the best fit for your research. If you are not sure, read the appropriate sections before making your selection.

☒ Life sciences ☐ Behavioural & social sciences ☐ Ecological, evolutionary & environmental sciences

For a reference copy of the document with all sections, see nature.com/documents/nr-reporting-summary-flat.pdf

# Life sciences study design

All studies must disclose on these points even when the disclosure is negative.

| | |
|---|---|
| Sample size | For experiments involving the use of human tissues from organ donors (all figures, extended data, and supplementary information) , sample size was variable depending upon the type of experiment due to the restricted availability of donor tissues of specific ages. For all imaging and flow cytometry analysis using these tissues, 10-21 donors were used for each tissue site analyzed. For the cell line experiments to measure phagocytosis, two experiments were performed containing 9-12 wells each and from each well 2-3 images were taken. |
| Data exclusions | We excluded two donors from the original analysis because re-review of the donor information sheet found mention of previous smoking. |
| Replication | Figures show data from multiple individuals. To assess age associated changes, we used multiple donors for each age group. For quantitative imaging analysis, 70-400 single 20X images were taken for each donor sample and stitched together for Figures 1d, 1e, 2a, 2c, 2d, 6a-d and extended data Figure 1 and 2c . (These experiments show images from the whole tissue. For Ki-67 and cytokine experiments in Figure 4e-f, 5a-f, and extended data 5b, 6a-f. 2-4 images were taken from each donor sample for analysis of cytokines produced by macrophages subtypes. Phagocytosis experiments were performed in two independent experiments with 9-12 wells per condition and for each well 2-3 images were taken. |
| Randomization | Donors were allocated to different groups according to their ages. |
| Blinding | The goal of the original study was a qualitative investigation of human lymph nodes, so it did not require any blinding to sample. During the course of these experiments we found significant quantitative differences in macrophages and lymph node structure as a function of particulates and age which are reported here. |

# Reporting for specific materials, systems and methods

We require information from authors about some types of materials, experimental systems and methods used in many studies. Here, indicate whether each material, system or method listed is relevant to your study. If you are not sure if a list item applies to your research, read the appropriate section before selecting a response.

### Materials & experimental systems

| n/a | Involved in the study |
|---|---|
| ☐ | ☒ Antibodies |
| ☐ | ☒ Eukaryotic cell lines |
| ☒ | ☐ Palaeontology and archaeology |
| ☒ | ☐ Animals and other organisms |
| ☒ | ☐ Human research participants |
| ☒ | ☐ Clinical data |
| ☒ | ☐ Dual use research of concern |

### Methods

| n/a | Involved in the study |
|---|---|
| ☒ | ☐ ChIP-seq |
| ☐ | ☒ Flow cytometry |
| ☒ | ☐ MRI-based neuroimaging |

## Antibodies

| | |
|---|---|
| Antibodies used | Brilliant Violet 421™ Rat anti-human IL-6 Antibody (clone: MQ2-13A5): BD Biosciences/ Cat#563279<br>Brilliant Violet 421™ anti-human CD36 Antibody (clone: 5-271): Biolegend/ Cat#336230<br>PerCP/Cyanine5.5 anti-human CD36 Antibody (clone: 5-271): Biolegend/ Cat#336224 |

Alexa Fluor® 488 anti-human CD36 Antibody (clone: 5-271): Biolegend/ Cat#336231
Alexa Fluor® 488 anti-human CD68 Antibody (clone: Y1/82A): Biolegend/ Cat#333812
Brilliant Violet 711™ anti-human CD11b Antibody (clone: ICRF44): Biolegend/ Cat#301344
Brilliant Violet 605™ anti-human CD163 Antibody (clone: GHI/61): Biolegend/ Cat#333616
Fixable Viability Dye eFluor™ 780: eBiosciences/ Cat#65-0865-14
Alexa Fluor® 700 anti-human CD45 Antibody (clone: 2D1): Biolegend/ Cat#368514
PE Mouse Anti-Human CD11c (clone: B-ly6): BD Biosciences/ Cat#560999
BV510 Mouse Anti-Human CD11c (clone: B-ly6): BD Horizon/ Cat#563026
APC anti-human CD169 (Sialoadhesin, Siglec-1) Antibody (clone: 7-239): Biolegend/ Cat#346008
PE/Dazzle™ 594 anti-human CX3CR1 Antibody (clone: 2A9-1): Biolegend/ Cat#341624
BV786 Mouse Anti-Human HLA-DR (clone: G46-6): BD Biosciences/ Cat#564041
Brilliant Violet 650™ anti-human CD80 Antibody (clone: 2D10): Biolegend/ Cat#305227
Brilliant Violet 650™ anti-human CD86 Antibody (clone: IT2.2): Biolegend/ Cat#305428
Brilliant Violet 421™ anti-human CD209 (DC-SIGN) Antibody (clone: 9E9A8): Biolegend/ Cat#330117
Human TruStain FcX™ (Fc Receptor Blocking Solution): Biolegend/ Cat#422302
APC Mouse Anti-Human CD8: BD Biosciences/ Cat#555369
Brilliant Violet 421™ anti-human CD19 Antibody (clone: SJ25C1): Biolegend/ Cat#363017
Brilliant Violet 421™ anti-human Ki-67 Antibody (clone: Ki-67): Biolegend/ Cat#350506
CD20 Monoclonal Antibody, Alexa Fluor 488 (clone: L26): eBiosciences/ Cat#53-0202-82
Alexa Fluor® 594 anti-Podoplanin/Lymphatic Endothelial Marker Antibody (clone: D2-40): Biolegend/ Cat#916608
Biotin anti-human CD3 Antibody (clone: HIT3A): Biolegend/ Cat#300304
PE/Cyanine7 anti-human CD64 Antibody (clone: 10.1): Biolegend/ Cat#305022
Brilliant Violet 421 Mouse anti-human TNF-a Antibody (clone: MAb11): BD Biosciences/ Cat#566275
Brilliant Violet 421 Mouse gG1, k Isotype (clone: X40): BD Biosciences/ Cat#562438
Brilliant Violet 421™ Rat IgG1, κ Isotype Ctrl Antibody: Biolegend/ Cat#400429
Brilliant Violet 421™ Donkey anti-rabbit IgG (minimal x-reactivity) Antibody: Biolegend/ Cat#406410
IFN alpha Polyclonal Antibody: Thermo Fisher/ Cat#PA5-115430
ARG1 Polyclonal Antibody: Thermo Fisher/ Cat#16001-1-AP
For antibody dilutions see methods.

Validation

All antibodies were commercially available and validated by manufacturers. CD19, Ki-67, podoplanin, Arg-1, IFNa and CD20 additionally validated for IHC/ICC/IF. The antibodies for cytokine analysis (IL-6, TNF-a, IFN-a and Arg1) checked with an isotype control.

## Eukaryotic cell lines

Policy information about cell lines

Cell line source(s)

THP-1:original source ATCC and obtained from Dr. Sankar Ghosh's lab- Columbia University.

Authentication

We performed the protocol for activation and differentiation of THP-1 cells to macrophages and performed flow cytometry of macrophages markers before and after activation, and imaged them as well to validate that they had the expected properties of THP-1 macrophages.

Mycoplasma contamination

The cells were not tested for mycoplasma.

Commonly misidentified lines
(See ICLAC register)

none

## Flow Cytometry

### Plots

Confirm that:

☒ The axis labels state the marker and fluorochrome used (e.g. CD4-FITC).

☒ The axis scales are clearly visible. Include numbers along axes only for bottom left plot of group (a 'group' is an analysis of identical markers).

☒ All plots are contour plots with outliers or pseudocolor plots.

☒ A numerical value for number of cells or percentage (with statistics) is provided.

### Methodology

Sample preparation

Following procurement, organs were transported to the laboratory and maintained in cold media supplemented with 5% FBS, penicillin/streptomycin, and glutamine (PSQ). LN tissues were dissected out from the lung or intestine, cleaned of fat and connective tissue, chopped into pieces, and incubated with RPMI (Fisher) media containing collagenase D (Sigma) and DNase (Sigma) for 60 minutes at 37°C. Cells were isolated with additional mechanical digestion and density gradient centrifugation with high yields of live cells, as previously described. LN cells were enriched for CD3- cells using biotin-conjugated anti-CD3 and EasySep™ Human Biotin Positive Selection Kit II (Stemcell Technologies). Following enrichment, LN cells were resuspended in FACS buffer (PBS/5% FBS/ 0.5% sodium azide) and stained for surface markers for 20 minutes in 4oC. For intracellular staining, cells were resuspended with Fix/Perm concentrate and incubated for 60mins at room temperature as indicated in the TONBO biosciences TF staining kit (CAT#TNB-0607-KIT). After cells were washed with perm buffer, they were resuspended in the perm buffer with the intracellular antibodies and incubated for 60mins at room temperature. Cells were

| | |
|---|---|
| | then washed and resuspended in FACS buffer and analyzed by flow cytometry using the BD LSRII (Becton Dickinson), and data were analyzed in FlowJo software. |
| Instrument | Becton-Dickinson LSRII instrument |
| Software | Flowjo: Tree Star/ https://www.flowjo.com/<br>Python: Python (2020)/ https://www.python.org/downloads/release/python-370/ |
| Cell population abundance | All cell population frequencies were clearly indicated. No sorting experiments were performed. |
| Gating strategy | We gated on Live, singlets and CD45+ cells for all the populations. Macrophage subsets gated as CD68+CD169-, CD68-CD169+, and CD68+CD169+. |

☒ Tick this box to confirm that a figure exemplifying the gating strategy is provided in the Supplementary Information.